UNIVERSIDAD CARLOS III DE MADRID

Plasma Diagnostics with Langmuir Probe: Fabrication, Theory, and Application

by

Gabriel González Saiz

Supervised by Xin Chen

A thesis submitted in partial fulfillment for the
degree of Aerospace Engineering

in the
Escuela Politecnica Superior
Bioengineering and Aerospace Engineering Department

September, 2016

Declaration of Authorship

I, Gabriel Gonzalez, declare that this thesis titled, 'Plasma Diagnostics with Langmuir Probe: Fabrication, Theory, and Application' and the work presented in it are my own. I confirm that:

- This work was done wholly or mainly while in candidature for a research degree at this University.
- Where any part of this thesis has previously been submitted for a degree or any other qualification at this University or any other institution, this has been clearly stated.
- Where I have consulted the published work of others, this is always clearly attributed.
- Where I have quoted from the work of others, the source is always given. With the exception of such quotations, this thesis is entirely my own work.
- I have acknowledged all main sources of help.
- Where the thesis is based on work done by myself jointly with others, I have made clear exactly what was done by others and what I have contributed myself.

Signed: Gabriel González Saiz

Date: September 29th, 2016

"Research is what I'm doing when I don't know what I'm doing."

Wernher von Braun

UNIVERSIDAD CARLOS III DE MADRID

Abstract

Escuela Politecnica Superior
Bioengineering and Aerospace Engineering Department

by Gabriel González Saiz

Supervised by Xin Chen

This project deals with the complete home-made manufacturing of Langmuir probes and later analysis of sets of data measured from a Helicon Plasma Thruster prototype under development. Three codes were implemented in Matlab to process the IV characteristics, General Method, which performs the fit for ions and the fit for electrons separately, EPFL method [Furno, 2012], fitting the entire region below the plasma potential at once, and Chen2001 algorithm, described in [Chen, 2001], and not used in the analysis due to failure in convergence. It is found that the EPFL method is more robust and easy to use than the General method. Also the monitoring of the plasma affected by the new thruster modifications, such as the new antenna configuration or the improved RF system, was possible thanks to this project.

Acknowledgements

First of all, I owe my deepest gratitude to my thesis advisor, Xin Chen. Not only for the constant close guidance throughout this new field for me but also for steering me in the right direction whenever she thought I needed it. Besides my advisor, I would like to thank Jaume Navarro for his willingness to help and insightful comments during the course of this project.

I must express my very profound gratitude to my parents and to my partner for providing me with unfailing support and continuous encouragement throughout this four years and the process of writing this thesis. This accomplishment would not have been possible without them.

Also, I am gratefully indebted to my bachelor friends for all the help given and all the good moments that did sweeten the pass through these studies.

Last but not least, I would particularly like to thank Guillermo, whose constant disponibility and will to help made possible the correct fabrication of the probes and my friend Charlie Alpha, who introduced me to the Latex world and helped me with the layout presentation of this thesis.

Contents

List of Figures

List of Tables

Abbreviations

IV	**I**ntensity **V**oltage
OML	**O**rbital **M**otion **L**imited
ABR	**A**llen-**B**oyd-**R**eynolds
BRL	**B**ernstein-**R**abinowitz-**L**aframboise
BNC	**B**ayonet **N**eill-**C**oncelman
LP	**L**angmuir **P**robe
GM	**G**eneral **M**ethod
EPFL	**E**cole **P**olytechnique **F**ederale de **L**ausanne
EM	**E**PFL **M**ethod
HPT	**H**elicon **P**lasma **T**hruster

Physical Constants

Speed of Light	c	=	$2.997\ 924\ 58 \times 10^{8}$ ms^{-2}
Boltzman Constant	k_B	=	$1.380\ 7 \times 10^{-23}$ J/K
Elementary Charge	e	=	$1.602\ 2 \times 10^{-19}$ C
Electron Mass	m_e	=	$9.109\ 4 \times 10^{-31}$ kg
Vacuum Permittivity	ϵ_0	=	$8.854\ 2 \times 10^{-12}$ F/m
Temperature associated with 1 eV	e/k_B	=	$1.160\ 4 \times 10^{4}$ K

Symbols

T	temperature	K
n	density	m^{-3}
U	angular frequency	$rads^{-1}$
m	mass	kg
r	particle position	m
v	particle velocity	m/s
I	current	A
V	potential	V
A	area	m^2

Subscripts

i	ion
n	neutron
e	electron
f	floating
p	probe
s	plasma
is	ion saturation
es	electron saturation

Dedicated to my family.

Chapter 1

Introduction

1.1 Plasma

Commonly, the term *plasma* does not appear much in our everyday lives. However, it is a true that plasma is a major research field that gets more and more important as advances take place. One of the most ambitious objectives is the controlled thermonuclear fusion, quite similar to that taking place in the stars. However, this goal seems yet far for the numerous complications and problems arising on the way.

One of the most clear and shortest definitions that could be given for plasma is ionized gas. However, being rigorous, all the gases have some degree of ionization, as described by the Saha equation, shown below,

$$\frac{n_i}{n_n} \approx 2.4 \times 10^{21} \frac{T^{3/2}}{n_i} exp\left(\frac{-U_i}{k_B T}\right) \ . \tag{1.1}$$

Then, for an ionized gas to be a plasma, the degree of ionization must be significant. These charge separation, expressed by positive ions and electrons, lead to a whole with totally different properties from those of a fluid and give rise to complex phenomena, such as electric and magnetic interactions involving the two species.

Once it is known what it is being studied, it is time to understand how the plasma is created. In order to obtain the degree of ionization to create plasma, it must be added the enough energy to the gas. However, it is not made simply by heating up a gas in a container, as the temperature of the container would also be high and be melted in the process. What it is done usually is heat a small amount of gas and drive a electric current through it. This addition of energy affects mainly the free electrons present in the hot gas, which begin to collide with the atoms and liberate new electrons. This

process cascades until the degree of ionization reaches the limit for the actual conditions [Goldston and Rutherford, 1995].

1.2 Plasma properties

In order to differentiate the plasmas between them, it must be known some quantitative parameters resuming the overall information of the plasma volume. Of course, these variables aim to give some prior information at a macroscopic level of the 3D studied volume. Similarly to the everyday fluids, the plasma is characterized by the density and temperature. Generally speaking, the density refers to the number of particles present and the temperature, to the energy these particles posses. It must taken into account plasma is composed of various different species and these properties are different for each species.

There are also important contributions to the definition of a plasma such as electric and magnetic fields. These modify completely the behaviour of the different particles confined inside the plasma but they are not going to be considered inside this work.

Throughout all the thesis the plasma is assumed to be un-magnetized, collision-less with Maxwellian distribution, so it is good to state it from the beginning. Regarding these properties, un-magnetized means there are no external magnetic field affecting the dynamics of the molecules and collision-less involves that the collisional mean free paths of the particles are larger than the characteristic lengths. A well-assumed fact is also the difference in temperature of the species, electron temperature is usually higher than that of the ions and neutrons $T_e >> T_i \approx T_n$.

1.3 Plasma diagnostics

The main aim of plasma diagnostics is to extract the information from the plasma created and thus find a way to describe that phenomena taking place in the laboratory.

By now there are many different types of plasma diagnostics, both intrusive and non-intrusive. Some examples of plasma diagnostics are the following [Hutchinson, 2002].

- Magnetic measurements
- Plasma particle flux measurements
- Plasma refractive index

- Electromagnetic emission from free and bound electrons
- Scattering of electromagnetic waves
- Neutral atom diagnostics
- Fast ions and fusion products

For the development of this project only electric probes are important, and are going to explain more in detail in the following paragraphs[Schrittwieser et al., 2005].

An important contribution to plasma diagnostics were the probes. The first probes were invented by Irving Langmuir in 1924-1926 while researching the new field of plasmas. After working some years on improvements for light bulbs, he focused his work on studying hot filaments at different gas environments. In 1924, he invented the diagnostic method for measuring both temperature and density with an electrostatic probe, now called a Langmuir probe [Mott-Smith and Langmuir, 1926] [Langmuir, 1960]

Regarding the types of probes, there are two main types of plasma probes, Langmuir probes and emissive probes.

- Langmuir probes consists of a single conductor inseted on the plasma which is biased to a potential range. In the following section these probes are explained more in detail [Chen et al., 1965].
- Emissive probes main working principle is the emission of electrons in order to obtain the information from the plasma. It consists of a small half-loop of tungsten wire connected to a power supply. A current is applied to the filament, heating it to the point where electrons are emitted. The classical way of proceeding is measuring the floating potential for a temperature sweep. The saturation of the potential indicates the value of the plasma potential [Hershkowitz, 2013] [Conde, 2011].

1.3.1 Langmuir probe

Langmuir probes are cold probes consisting of a small electrode of various shapes which is inserted into the plasma and externally biased with respect to the plasma potential. However, since the plasma potential is not directly accessible, the bias has to be applied with respect to the external reference electrode or ground. The term cold refers to the activity of the probe, it only passively registers the charge fluxes towards it, but does not emit particles. These currents depend on the surrounding plasma, on the probe bias Vp, on the shape of the electrode, and on the magnetic fields, which will not be regarded in this thesis.

Generally speaking, electric probes measure local plasma parameters by using stationary or slow time varying electric fields to emit or collect charged particles from the plasma. The process of measuring works the following way. The probe is polarized to a potential V_p. A current is drained from the plasma to the probe for the difference in potential between both elements, probe and plasma. To obtain a complete set of data regarding electrons and ions, the potential given to the probe is swept from very negative values to high positive potentials. The result from this procedure is the IV characteristic (Current - Voltage) in which it is shown the voltage at which the probe was polarised and the current extracted from the plasma. This current is composed of two main contributions, the ion and the electron current: $I = I_i + I_e$. Due to their difference in charge, they also have different sign. An example for an IV curve is given in Figure 1.1.

The plasma parameters are then derived from this data set following different ion collection theories concerning different plasma regimes.

As exposed by Figure 1.1, there are three clear regions depending on which potential is the probe biased at [Merlino, 2007].

For very negative bias voltages $V_p < V_s$ ions are attracted and electrons are repelled. The drained ion current from the plasma is limited by the electric shielding of the probe and Ip decreases slowly towards more negative potentials. The current collected mainly due to ions is called ion saturation current.

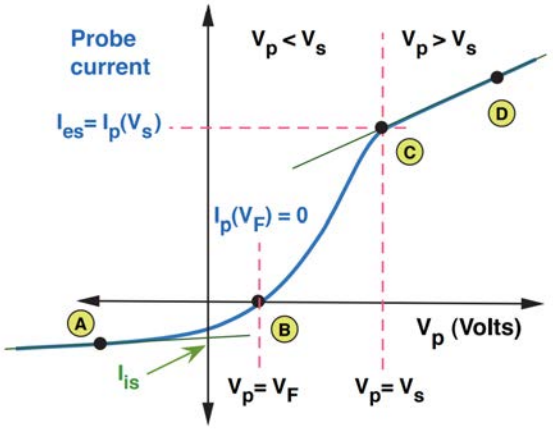

FIGURE 1.1: Ideal IV characteristic for a Langmuir probe [Conde, 2011]

For very positive probe potentials, $V_p >> V_s$, the ions are repelled and the electrons are the attracted charges. In this case the electrons are responsible for the electric shielding of the probe and $I_p \approx I_{es}$ is called the electron saturation current. Too many real effects take part in the electron saturation region so it is usually discarded to obtain reliable plasma parameters.

In between these two regions, the currents from both species are important. The bias potential V_f where $Ip = 0$ is the floating potential (point B in Fig.1.1) where the contributions of the ion and electron currents are equal.

1.4 Plasma emitters

It will be referred to plasma emitters to those devices able to create plasma regardless of its purpose. The following section introduces briefly three plasma emitters even though the device most data come from is the Helicon Plasma Thruster.

The simplest way to produce and measure plasma is creating a glow discharge plasma into a glass tube. An electric discharge, usually produced by a high DC voltage, is applied between both ends of the glass tube and a the corresponding discharge current can be measured if a probe is positioned inside the tube.

The hollow cathode electron emitter is another device to produce plasma. It consists of using an arc to dissociate some material from a surface. These particles, electrons normally, later bombard the gas entering the system through the cathode, which is highly ionized. The gas source then becomes a highly ionized plasma source from which the plasma is directed to the anode.

In the case of the Helicon Plasma Thruster, radio frequency radiation is used to break down the gas structure and maintain the plasma generation. The device is made up of a cylindrical chamber, a radio-frequency antenna, RF subsystem, a feeding system and a set of electromagnets around the chamber. First, a wave is emitted by the antenna to the plasma. The energy from this wave is absorbed mainly by the electrons, which later bombard the neutral gas producing the plasma. The plasma is then guided and its particles are accelerated by the action of the electromagnets coiled around the chamber [Navarro-Cavallé et al., 2013]. A picture of a working HPT is given in Chapter 4.

1.5 Project objectives

The tasks of this project have been chosen considering the current situation of the plasma lab team. A new plasma laboratory has been prepared at the University Carlos III de Madrid and it is needed a diagnostic system to measure the plasma from a thruster in a reliable way. In addition, the results must be analysed to monitor the development of the propulsion device. Given those circumstances, the main established aims have been the following:

1. Manufacture a hand-made Langmuir probe and the necessary cables for the data extraction.
2. Implement post-process procedures to obtain key plasma information from the IV curve measured.

3. Analyse the data for different configurations of the plasma emitters.

While it is true that the objectives of the project have been unchanged throughout its course, the data processing procedures were reconsidered during the project.

1.6 Document structure

The following section presents a brief introduction of the contents of the document divided in chapters, excluding the introduction, already past.

- The theoretic background, comprised in **chapter 2**, introduces the kinetic theory and enters deeply into the planar collection theory. It also summarises later cylindrical theories such as OML, ABR, and BRL.
- **Chapter 3** explains in detail how the probes were manufactured by hand. The list of materials used and a step-by-step procedure is given for two different cases, an initial probe model and its younger sister, the one mounted for the experiments.
- In **chapter 4** it is set the background of the experiment and it is included a brief description of the vacuum chamber and plasma emitters used. It is also explained the probe disposition.
- **Chapter 5** elaborates on the process codes that result in the plasma parameters. A short description of the procedure followed by each code inputs and outputs and how the user should interact with it.
- **Chapter 6** resumes the analysis output of the data obtained from the probes with the implemented codes and the comparison between the results of the codes for different conditions of the plasma.
- The regulatory and socio-economic framework is comprised in **chapter 7**, where the budget for this project is also included.
- Finally, in **chapter 8**, conclusions are drawn mainly on the process procedures and on the results obtained from the analysis of the data. Some guidelines are given for future works too.

1.7 Project schedule

The planning of the project is shown in the next figure. The most important tasks and the time devoted for them are represented in the Gantt diagram.

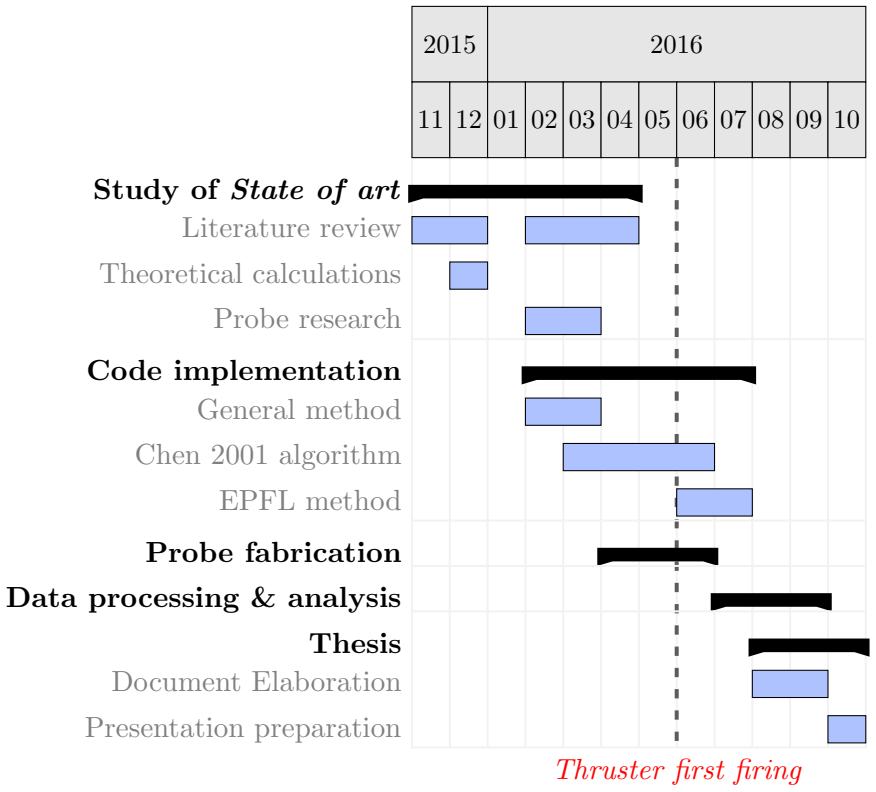

FIGURE 1.2: Timeline for the project tasks

Some remarks concerning the schedule of the project that may need to be clarified are the following.

- There is a cut on the work done on January, due to the ordinary exams from first semester.
- Even though some probes were already manufactured by April, the helicon thruster was not fired until the end of May. This fact explains the time taken to start processing the data.
- The data processing and analysis concerns both the individual processing of each code and the method comparison procedure for all the data gathered.

Chapter 2

Theoretical Background

Once it was introduced the concept of plasma and it was given a broad idea about plasma diagnostics, it is necessary to go through the theoretical background governing the physics behind those measurements. The aim of the following sections is to present the state of art of the collective theories which will go from the simplest theory, the planar approach, up to one of the most valid and modern theories.

2.1 Kinetic theory

To understand the behaviour of the plasma as a whole, first it must be studied the units conforming it. Any particle present in a plasma can be described by a position vector and a velocity vector conforming the phase space [Miyamoto, 1997]:

$$\begin{cases} \mathbf{r} = x\mathbf{i} + y\mathbf{j} + z\mathbf{k} \\ \mathbf{v} = v_x\mathbf{i} + v_y\mathbf{j} + v_z\mathbf{k} \end{cases} \tag{2.1}$$

For multi-particle systems, all the elements are considered by the distribution function $f(\mathbf{r}, \mathbf{v}, t)$, which is defined the following way:

$$f(\mathbf{r}, \mathbf{v}, t)d\mathbf{r}d\mathbf{v} = dN(\mathbf{r}, \mathbf{v}, t) \tag{2.2}$$

Based on the dependence of the distribution function on $\mathbf{r}$ and $\mathbf{v}$ the definition of the distribution function varies. If $f(\mathbf{r}, \mathbf{v}, t)$ is independent of the direction of $\mathbf{v}$ or not, the distribution is *isotropic* or *anisotropic* respectively. A well-assumed case for simple theoretical approaches is the plasma in *thermal equilibrium* which implies an homogeneous, isotropic and time-independent distribution function.

An important example of velocity distribution function for a plasma in thermal equilibrium is the Maxwell-Boltzmann distribution, also called Maxwellian. It can be described by a simple Gaussian spread of velocities with the half-width being related to the gas temperature, as shown by 2.3.

$$f_{Maxw}(\mathbf{v}) = n\left(\frac{m}{2\pi k_B T}\right)^{3/2} exp\left(-\frac{m\mathbf{v}^2}{2k_B T}\right) \tag{2.3}$$

The macroscopic variables or plasma parameters are obtained by taking appropriate moments of the distribution function [Goldston and Rutherford, 1995].

One of these, which is calculated later for the analysis, is the number density, or density of particles, and is defined by:

$$n(\mathbf{r}, t) = \int f(\mathbf{r}, \mathbf{v}, t) d\mathbf{v} \tag{2.4}$$

The mass or charge density can be derived from this expression if multiplied by the unit mass or charge respectively.

On the other hand, the temperature is a property which is related to velocities, thus, kinetic energy, and pressure. The dependence on the velocity of the particles is shown below:

$$v = \sqrt{\frac{2k_B T}{m}} \tag{2.5}$$

Form 2.5 it can be deduced that the temperature is directly proportional to the average kinetic energy of the particles present in the plasma. The following expression shows the average kinetic energy in 3D meaning then each degree of fredom possess $\frac{1}{2}k_B T$ energy.

$$E_{av} = \frac{3}{2}k_B T \tag{2.6}$$

Regarding the pressure relation, electrons and ions contribute equally to the plasma pressure:

$$p = \sum_{\alpha} n_\alpha k_B T \tag{2.7}$$

Given the previous relations, it is understood why in plasma physics the temperature units are those of energy, eV, coming from $k_B T$. Thus, $1eV$ temperature corresponds to

$$T = e/k_B \approx 11600K$$

2.2 Planar model

The planar model is the simplest of the theories for plasma diagnostics and it is deeply explained in the next section. It consists mainly on a planar geometry probe located inside a plasma, reducing then the problem to only one dimension [Chen et al., 1965] [Goldston and Rutherford, 1995] [Merlino, 2007] [Hershkowitz, 2013] [Conde, 2011].

The planar approximation consists of assuming that the sheath dimensions are small compared to the probe dimensions. However, in a planar model, 2.3 is reduced to a 1D problem, simplifying the algebra but losing information of the other dimensions. This step could not be taken if the distribution function is known to be different than isotropic.

Having introduced the term sheath, it is crucial to explain the Debye length. It is essentially the maximum distance at which a charged particle is affected by the electric field of another particle of opposite charge, and it is described by 2.8. It becomes relevant when talking about the sheaths created around the probe for very negative or very positive potential bias.

$$\lambda_D = \sqrt{\frac{\epsilon_0 k_B T_e}{n e^2}} \tag{2.8}$$

A well-assumed distribution function is that of non-drifting Maxwellian particles that is expressed by the following equation,

$$f(x, v, t) = n_e \left(\frac{m_e}{2\pi T_e}\right)^{\frac{1}{2}} exp\left[-\left(\frac{m_e v^2}{2T_e}\right)\right] . \tag{2.9}$$

The IV characteristic presents three different regimes depending on the probe potential, see figure 2.1. Also, as explained before, there are two important potential values which divide the regimes, the floating potential and the plasma potential. The floating potential is just the point at which both currents, from ions and from electrons, cancel each other. The plasma potential, in contrast, is more interesting. At the plasma potential, the probe potential is equal to that of the plasma, meaning the current drained is mainly due to the random flux of particles. Therefore, the ion or electron current are obtained from equation 2.4.

$$I_{i,e} = \frac{1}{2} A_p n e \sqrt{\frac{2 k_B T_{i,e}}{\pi m_{i,e}}} \tag{2.10}$$

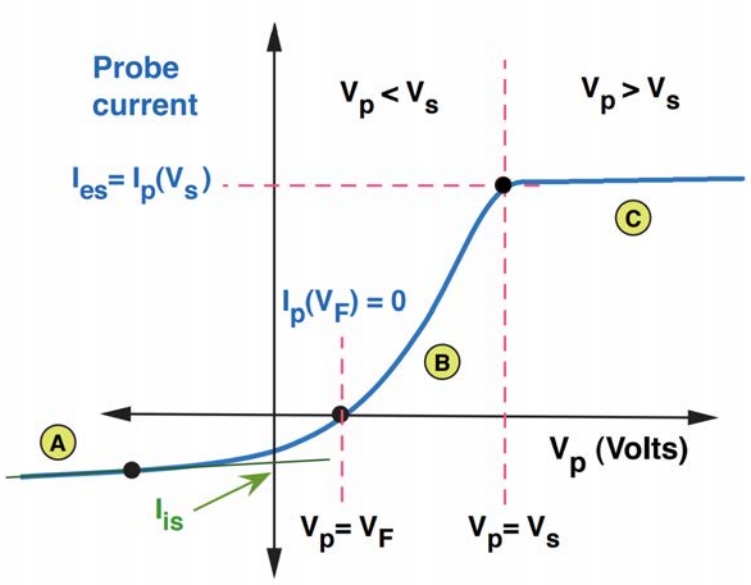

FIGURE 2.1: IV characteristic for a planar Langmuir probe

Usually the current measured contains the contributions of both electrons and ions, $I = I_e + I_i$, having each of them opposite sign. In the majority of the cases, the current at the plasma potential is positive, meaning the ion current is negligible compared to the electron contribution. The reason for this fact is the larger mass of the ions and their lower energy.

Regime C

When the probe potential is larger than the plasma potential, that is, more positive, electrons are accelerated and ions repelled. This repulsion of positive ions implies the appereance of a positive sheath around the probe. It may seem that the sheath enhance even more the atraction of the electrons, but if the sheath is thin compared to the probe dimensions, the electron current gets saturated and may remain constant even when increasing the potential. However, if the sheath expands, the effective collection area increases. Now, the sheath area is no longer equal to the probe area, which means, there is no longer electron saturation.

Due to this real effect and much others taking place at this high potentials, this region is usually avoided when obtaining information about the plasma.

Regime A

In the case of very negative probe bias, electrons are repelled and a negative sheath is formed. It could be reasonable to expect a similar behaviour for the ions than for the electron saturation region, but in fact it does not. One of the assumptions made is that the temperature difference is high, $Te >> T_i$. This involves that the negative pre-sheath

created by the electrons is strong enough to accelerate the ions up to the Bohm velocity, which they enter the sheath with.

$$v_B = \sqrt{\frac{k_B T_e}{m_i}} \tag{2.11}$$

Assuming quasineutrality and given that the repelled electron density at the sheath is $n_{e0} = e^{-1/2} n$, the ion saturation current can be deduced the following way:

$$I_{i,sat} = -A_p n_{i0} e = -A_p n_{e0} e = -e^{-1/2} A_p n e \sqrt{\frac{k_B T_e}{m_i}} \tag{2.12}$$

Regime B

The intermediate regime B is considered the range between the two saturation current ranges, A and C. As the probe potential is yet lower than the plasma potential, a negative sheath appears around the probe due to the repulsion of some electrons. The electrons that are not repelled, have the enough energy to reach the probe and contribute to the current measured. Then the current can be calculated the same way than in the saturation case but imposing a minimum velocity for the electrons, v_{min}, that account for the sheath. According to the Bohm criterion, the velocity associated to the necessary energy is $v_{min} = \sqrt{\frac{k_B T_e}{m_e}}$, being the minimum energy, $k_B T_e = 2e(V_s - V_p)$.

$$I_e(V_p) = e A_p n \int_{v_{min}}^{\infty} \sqrt{\frac{m_e}{2\pi k_B T_e}} exp\left(-\frac{m_e v^2}{2 k_B T_e}\right) dv = I_{e,sat} exp\left[\frac{-e(V_s - V_p)}{k_B T_e}\right] \tag{2.13}$$

Then, it can be seen that when subtracting the ion current from the total current and plotting the resultant in a semi-log graph, I_e vs V_p, it should appear a linear region corresponding to the pure exponential of 2.13. This way the electron temperature value can be extracted knowing the slope of that straight line is $e/k_B T_e$ in K and $1/T_e$ in eV.

At this point, an estimation of the plasma potential can be done in case of having no other way to obtain the value. This calculation implies the floating potential and the particularity of having the two contributions of the same magnitude. Then, merging 2.12 and 2.13 it is found the next expression,

$$V_s - V_f = \frac{1}{2}\left[ln\left(\frac{2\pi m_e}{m_i}\right)\right]\frac{k_B T_e}{e} \tag{2.14}$$

2.3 Cylindrical and spherical models

The problem changes when the probe cannot be assumed as planar due to the probe shape or finite probe size. A new dimension must be considered, as well as all the new theoretical corrections to account these effects. The following sections elaborate briefly on cylindrical orbital theories without entering deeply into the equations.

2.3.1 Mott-Smith and Langmuir theory

The theory developed by Mott-Smith and Langmuir was one of the first models describing the plasma behaviour around a collector [Mott-Smith and Langmuir, 1926]. The main objective of the work done was to obtain the theoretical current collected when biasing the probe at a certain potential. The potential profile between the plasma and the probe was not taken into account, and thus the sheath structure was not fully considered. This model only considers the 2D problem so the end effects of the probes are totally disregarded.

A key decision done by Smith and Langmuir was to develop the collected current expression taking into account the sheath radius, that is normally unknown at this step. To fully define the ion current, two limiting cases arose, the sheath is either very large compared to the probe size, or very small.

2.3.1.1 Thin Sheath Limit

If the surrounding sheath is considered very small compared with the geometry of the probe, it is consequently assumed that the probe radius is much larger than the Debye legth. This does not lead to a surprising result as the collected current is independent of the potential imposed to the probe because all the ions crossing the sheath are collected. This approach is similar to the planar theory [Tejero del Caz, 2016].

2.3.1.2 Orbital Motion Limit

In the case of the Orbital Motion Limit condition, the sheath is large compared to the probe radius. This means the Debye length is much larger than the probe radius and the ions have a totally different behaviour inside the sheath, governed by orbital motion.

After performing all the necessary calculations, it is concluded that the ion current does depend on the potential at which the probe is biased.

2.3.2 Bernstein-Rabinowitz-Laframboise theory (BRL)

The theory of Bernstein and Rabinowitz can be considered an extension of the Mott-Smith and Langmuir theory accounting for the potential structure of the sheath [Bernstein and Rabinowitz, 1959]. Roughly, they solved the Botzmann's equation to obtain the density across the potential distribution and insert it into the Poisson's equation to obtain the potential distribution and finally calculate the collected current.

However, they performed the calculation for a mono-energetic distribution function so Laframboise followed the same procedure as Berstein and Rabinowitz but with a fully Maxwellian ion distribution almost a decade later [Laframboise, 1966].

2.4 Real effects of probes

This section deals with some real effects that slightly modify the ideal IV curve and must be considered in order to obtain the real plasma parameters when analysing the curve. This brief introduction is exclusively qualitative and its objective is to make known some of these real effects that complicate the analysis of probe results. More detailed explanations can be found on [Chen et al., 1965].

A phenomenon affecting the acquired data is the probe contamination. It may happen that a layer of foreign particles different from the metal deposit on the surface of the probe. This layer act as a additional resistor difficult to determine which decreases the collected current [Hershkowitz, 2013]. This effect can even be intensified with low temperatures plasmas. There is not an easy way to account for this effect quantitatively but it must be done experimentally. The probe must be kept under electron or ion bombardment by a large positive or negative bias in order to eliminate the contaminant surface.

Other effect that can not be solved easily by data processing is secondary emission. When the probe is biased at large negative potentials, the heavy ions may liberate electrons when impacting the probe. These electrons may be emitted due to the negative potential of the probe, implying then a secondary emission of electrons and being shown in the IV curve as a false increase in the ion current. It can be avoided when selecting the material for the probe collection core, which must be a low emission material.

A common issue is the perturbation of the plasma by the probe itself and its shield. Some side effects of measuring the plasma can be lowering the temperature of the electrons due to collisions with ions detached from the probe shield and the decrease of plasma density in the probe neighbourhood due to the collection of ions by the probe shield.

Chapter 3

Probe Fabrication

One of the multiple tasks of this thesis was to manufacture hand-made Langmuir probes in order to test them and validate and analyse the data obtained.

The next points show the first prototype of the Langmuir probe, how was it fabricated and what changes were performed to the model to improve the easiness in installation and operation.

3.1 Initial probe design

From the beginning, the model of the probe consisted of three main parts: collection area, protected body and connection part [University of Michigan]. The collecting length is determined by the plasma it is going to be immersed in. Then, it is needed a separation between the collecting spot and the connection for two main reasons. First, the plasma being diagnosed must not be disturbed by anything, even other parts of the probe. The distance of interference is the Debye length, as previously seen, and depends on the plasma. Secondly, the joint with the cable usually imply other materials not so well prepared for high temperatures. Finally the connection with the cable is done by means of crimping and must be also protected.

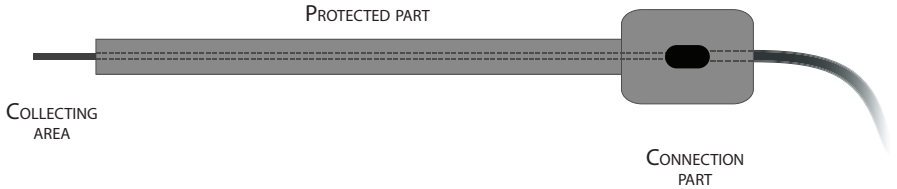

FIGURE 3.1: Sketch of a general probe parts

The extreme conditions present inside the plasma volume determine the characteristics of the materials used in the fabrication of any probe. The most important part of a probe is the collecting surface, it must be able to withstand the constant bombardment of particles without being eroded or damaged. That is the reason why the core must be made up of a material with a high melting point but also with a high electric conductivity to measure faithfully the incoming current; in this case tungsten was chosen.

Regarding the encasement of the main body, a refractory ceramic material, aluminium oxide, was preferred. Again, the material must have a high melting point to resist the high temperature without breaking or fracturing. Also it should be long enough for the collecting head to be inside the plasma and the other end outside of it.

The connection between the tungsten and the cable is more critical than it may appear at the beginning. Soldering both elements is not enough to ensure the integrity of the attachment, so crimping is mandatory. However, a problem may arise when trying to crimp a tungsten rod with the cable. The rod is rigid and brittle and the force exerted on the crimping process might brake the part. The most straightforward alternative is using tungsten wire, which is more flexible and can be bent carefully to improve the contact surface.

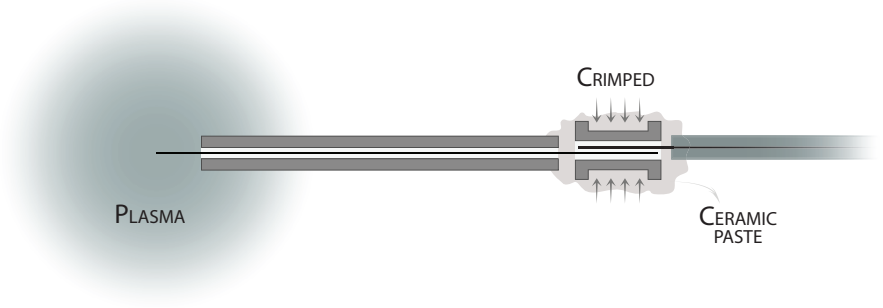

FIGURE 3.2: Sketch of first initial probe model

The next two points enumerate the materials and describe the procedure followed to build the first probe.

3.1.1 Materials

The materials used for the first Langmuir probe are the following:

- Tungsten wire
- Alumina tube
- Ceramic paste

- Electric cable
- Soldering wire
- Short metal tube for crimping

3.1.2 Procedure

Next the steps, which should be followed rigorously in order to achieve a successful probe, are described below.

1. Prepare all the materials and the necessary tools. The workspace should be clean and tidy.
2. The first step is to cut the tungsten wire or rod. It must be considered the length of the ceramic protection tube, the exposed length and some extra length to establish the connection with the cable. As this last part may vary during the crimping process, it may be needed to cut again the probe tip afterwards.
3. Next, the tungsten must be crimped to the cable that will lead the information out of the chamber. This can be done easily with the help of a little metal tube embracing both materials. The crimping is performed with a specific tool called crimp tool. Note that there are many different crimp tools with variable crimping diameters. In case of not using a suitable crimp tool, the tube could end crushed or loose, both cases resulting in a wrong connection. In addition, once the group is crimped, it can be soldered to increase the contact surface between metals and improve the connectivity.
4. Prepare the ceramic paste following the instructions of the supplier.
5. Insert totally the tungsten core through the ceramic tube and apply ceramic paste around the crimped tube until both non-metal ends are reached with the help of a small stick or scraper. Be sure to cover all the metallic area exposed in order to prevent capturing additional particles.
6. Once the ceramic paste has dried and cured, cut the excess of collecting length at the end of the probe if necessary.
7. Polish the end until the shape of a cylinder is achieved. This last step may not be necessary is the cutter was suitable enough.

3.2 Final probe design

The first probe was manufactured long before a standard was met for the probe mounting system inside the chamber. when the thruster ignition was already feasible, decisions on the probe connections had to be made, and it was opted by a BNC connection to the cables, simplifying the mounting process and being suitable also for emissive probes. Once the connection between the cable and the probe core was decided to be changed, the fixing mechanism for the probe components was reassessed.

Ceramic paste main inconvenience was the lack of opportunity to examine the probe connection in later inspections. Note that even though the tungsten core was crimped and soldered to the BNC male connector pin, the reiterative pressurisation and de-pressurisation process could weaken the connection forcing the probe to be opened and repaired. For that reason, ceramic paste was discarded for this model and a washer was used instead. The material of the washer is not as critical as the core or the protection because it was not supposed to suffer the effect of the plasma directly. As sketched by figure 3.4, the body of the probe is long enough to avoid introducing the whole assembly inside the plasma. Otherwise, in case the probe is totally submerged, the washer should resist the high temperature of the plasma and be as resistant to ablation as possible.

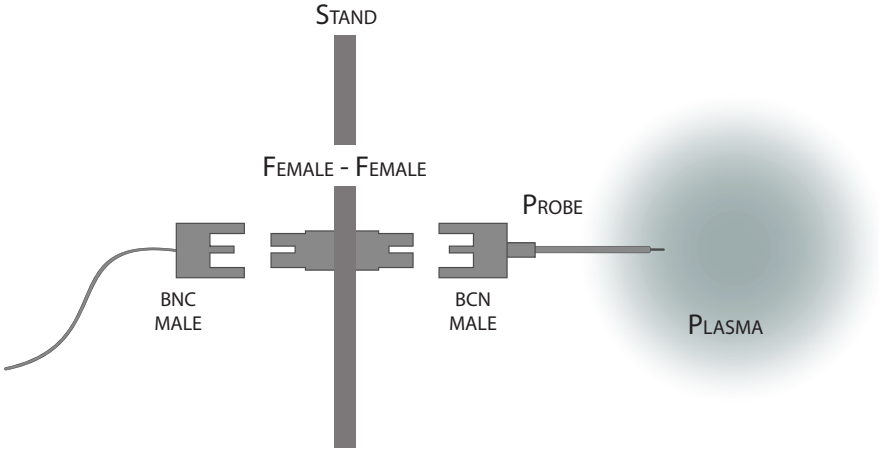

FIGURE 3.3: Sketch of BNC connections arrangement in probe mounting. Not to scale.

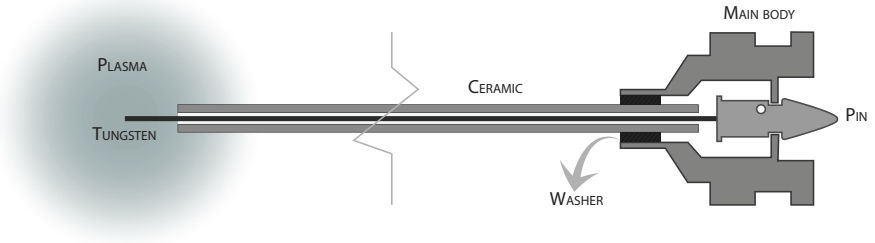

FIGURE 3.4: Sketch final probe model. Not to scale.

3.2.1 Materials

The materials used for the improved Langmuir probe are the following. It was included the cable connecting the probe to the chamber, but it was discarded the pin used for the connection of the end of the Kapton cable.

- Tungsten wire
- Alumina tube
- Fixing washer
- BNC adapter Female/Female
- 2 x BNC male connector
  - Crimp ferrule
  - Contact pin
  - Main body
- Kapton cable
- Soldering wire

(A) Tungsten wire coil (B) Alumina tube casing (C) BNC male connector elements (D) Kapton cable

FIGURE 3.5: Picture of materials used for Langmuir probe fabrication.

3.2.2 Procedure

1. Prepare all the materials and the necessary tools. The workspace should be clean and tidy.
2. Begin taking the tungsten wire and the BNC male connector pin. The idea is to crimp the hollow end of the pin around the tungsten wire. To do so, the wire can be rolled up to an auxiliary cylinder due to its thinness, as shown in figure 3.6. This may be a difficult task by hand considering the rigidity of the tungsten metal.

For this project this was done with a specific electrician device used to coil thin wires around a small pins.

FIGURE 3.6: Sketch of coiled tungsten and pin assembly

3. Once the roll of tungsten is inserted inside the pin, proceed to crimp with the crimp tool. It may happen that the pin is not specific for crimping; in such case apply force carefully on the most suitable diameter hole until the tungsten is secured strongly enough.

4. Again, it may be useful to solder the whole joint to increase the contact surface. Be careful not to overflow with soldering wire the guide marks of the pin used to fitting in the main body of the BNC connector.

5. Insert completely the alumina tube and cut the tungsten wire with the desired collecting length. It is important to use the right tool as it strongly affects the later polishing of the tungsten.

6. Polish the end of the tungsten wire until the shape is perfectly cylindrical. In case the wire is very thin to be checked by eye, the use of a microscope is recommended. This step may not be necessary if the cutter was suitable enough.

7. Assemble the main body of the BNC connector; a click must sound to indicate that the pin is correctly placed. Afterwards slide the washer around the probe body and fit it in the annular hole between the protection tube and the BNC body. A thermoretractable tube can be wrap around the washer position for a stronger fastening.

FIGURE 3.7: Manufactured probe sample

3.3 New designs and future work

The main drawback of the created Langmuir probes is their fixed lengths, and so their fixed collecting area. This means a numerous number of probes must be built in order to change these geometry parameters to adapt the most suitable collecting area to the actual plasma regime. Moreover, if this process can be done in vacuum automatically, the life of the probes would be increased. However, it is true that this automatic system imply more complexity. One of the next steps to be taken in this part of the experiment would be to manufacture a probe with variable length.

A more feasible extension of this fabrication part is the manufacturing of a radio frequency compensated Langmuir probe. The effect of the oscillating plasma potential on LP is considered an issue when interpreting the data, as the electron temperature can be overstimated [Sudit and Chen, 1994]. Given that the Helicon thruster plasma generation is done by RF, a compensated LP could correctly measure the temperature of the plasma.

Chapter 4

Experiment Set-up

Once the probes were totally manufactured and ready to be tested, the data acquisition took place. Three different probes were fabricated and mounted simultaneously, even though only one was measuring at a time. The geometry of the three vary between each other, as shown by table 4.1, as it was planned to have three different collecting surfaces in order to adapt the probe to the actual plasma delivered by the thruster.

Probe Name	Probe Length [m]	Probe Radius [m]	Collecting surface [m2]
A	5e-3	6.35e-05	1.9949e-06
B	3e-3	6.35e-05	1.1969e-06
C	3e-3	1.27e-4	2.3939e-06

TABLE 4.1: Probes dimensions

The distance between them was enough to avoid any interference, as shown in figure 4.3. The plasma was expected to have an electron temperature of around 5 eV and a density of $10^{15}m^{-3}$, meaning a Debye length of 0.5 mm approximately, much lower than the distance between the probes.

The first stand was simply a structure with clamps grabbing the probes in the correct position. Is under development a more sophisticated stand meeting the standard of the BNC connectors of the probes.

FIGURE 4.1: Vacuum chamber at EP2 facilities

FIGURE 4.2: Probe mounting set-up for the Helicon Plasma Thruster

Unluckily, due to the fact that the tungsten wire was supplied coiled, the thinner probes bent slightly over time. Also, an accident affected one of the probes in a maintenance operation of the thruster. Right now only two of the probes are operative even though more specimens are to be manufactured.

A fourth probe was manufactured, having modified the part of the connection. Instead of the standard BNC connector, the tungsten wire was crimped directly to a Kapton cable, as for the case of the initial probe model, but replacing the ceramic paste with thermoretractable tube to isolate it from chamber. This way, in case the connection needs to be checked, the thermoretractable plastic is cut and removed and later replaced easily.

The experiment is performed at the experimental facilities of the EP2 research group in the Universidad Carlos III de Madrid.

FIGURE 4.3: Probe mounting set-up for the cathode

The vacuum chamber used is certified by Leybold Oerlikon and is optimized for the testing of low-mid power thrusters up to 2 kW and 100 sccm. This stainless steel chamber has the following features:

- Chamber dimensions:
  - Diameter: $1.5\,m$ (inner)
  - Length: $3.5\,m$
  - Volume: $6.2\,m^3$ (approx.)
- Vacuum performance:
  - Continuous operation at $< 2 \times 10^{-5}$ mbar at 20 sccm of Ar or Xe
  - Total pumping speed 37000 l/s Xe
  - Ultimate vacuum pressure $< 10^{-7}$ mbar
- Fully oil-free vacuum system:
  - Rough vacuum dry pump, Leyvac LV80 (80 m/h)
  - 2 magnetically levitated Turbomolecular pumps, MAGW2.200iP (2000 l/s each)

– 3 Cryopanels, Leyvac 140 T-V (adaptable to Xe or Ar)

The plasma generators used to test the probes were two.

- A **Helicon Plasma Thruster** developed cooperatively by SENER Ingeniería y Sistemas and EP2-UC3M and run mainly on argon and xenon propellants. Some important characteristics of the HPT are the following:

Physical characteristics		Operating range	
Ionization chamber	Length: 10-25 cm (Nominal 15 cm) Inner radius: 1.5 cm	Mass flow rate	15-60 sccm (Nominal 50 sccm)
Antenna	Half-helical; Length: 7.5 cm	Power input at RF generator	200-1000 W (Nominal 800 W)
Internal field generator	Two copper coils on spool; 435 turns each Mean coil radius: 42.5 cm	Magnetic field in chamber	0-600 G (Nominal 400 G)
Magnetic nozzle	Single copper coil on spool; 143 turns Mean coil radius: 6.1 cm	RF frequency	6.78 - 27.12 MHz (Nominal 13.56 MHz)

TABLE 4.2: Home HPT characteristics

- A **Hollow Cathode Plasma Electron Emitter** with 5 A operating current.

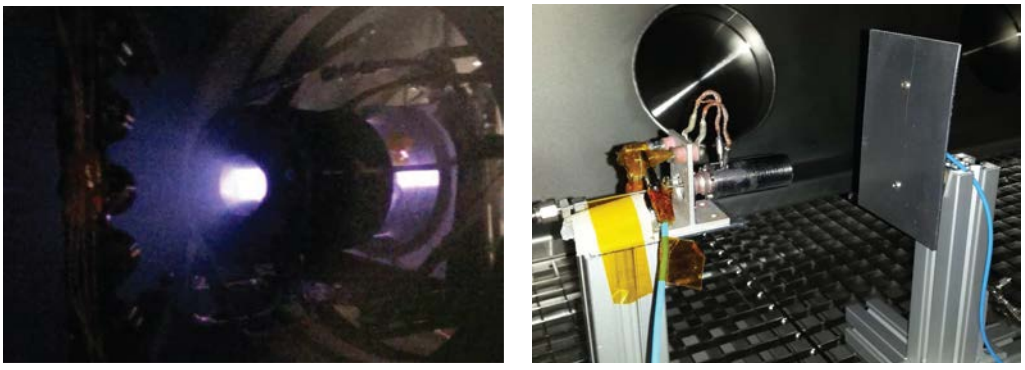

(A) Helicon plasma thruster prototype (B) Hollow cathode device

FIGURE 4.4: Plasma emitters tested

For the data acquisition task, two possible solutions were available.

The most simple one was to build an easy circuit as the one sketched in figure 4.5. The idea is to bias the probe at a potential V_b including a known resistance on the line. The actual potential of the probe is measured by the voltmeter V_p and the current collected by the probe is deduced from the measurement of the voltage at the resistance R_m by the voltmeter V_R.

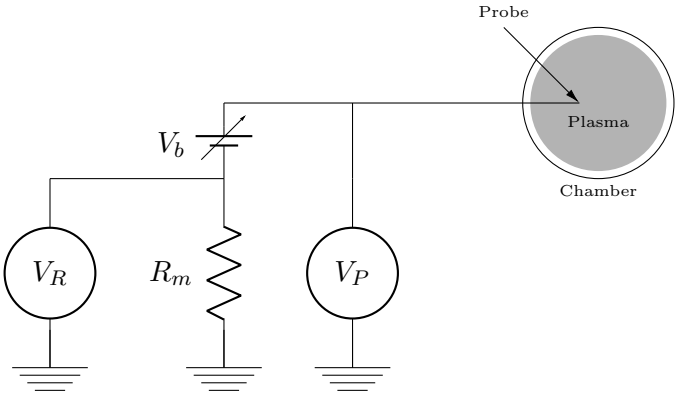

FIGURE 4.5: Schematic for simple experimental set-up for measurements with Langmuir probe.

A clear disadvantage of this setup is that the data must be recorded by hand making experimental time too large and the possible uncertainty dangerous.

A more expensive option, but with a higher reliability and precision is an electrometer. Usually these devices already gives the current passing through the probe, without the need of correcting it. In addition, they present some functionalities such as smoothing, that improve the quality of the curve and saves processing time by outputing directly the set of data in a text file.

Finally, the data acquisition was done by an electrometer from Keithley. The model used is the 6517B, which is a $6\frac{1}{2}$ digit Electrometer/high-resistance system with the following measurement capabilities and more [KEITHLEY]:

- DC voltage measurements from $1\mu V$ to $210V$
- DC current measurements from $10aA$ to $21mA$
- Charge measurements from $10fC$ to $2.1\mu C$
- Resistance measurements from 10Ω to $210P\Omega$
- Built-in V-Source: The 100 V range provides up to ±100V at 10 mA, while the 1000 V range provides up to ±1000 V at 1 mA.
- Data storage (50,000 points)
- Single button zeroing (REL)
- Built-in math functions
- Filtering: averaging and median
- Built-in test sequences

Chapter 5

Algorithm Description

During the course of the thesis, three different procedures have been studied and implemented. Two of them, General Method and EPFL Method, this last referring to the method followed by the Ecole Polythecnic Federale de Lausanne, are detailed below and whose results are discussed and compared on the Chapter 6. On the other hand, the third method, explained in [Chen, 2001], was studied and implemented but the results obtained from it did not match the other methods. For that reason it was decided to be discarded from the analysis results and comparisons. However, it should be included into future work the further studies about this procedure, particularly checking the convergence of the algorithm.

The software in which they are implemented was decided to be Matlab, [Mathworks], for its engineering use. The main advantage is the huge database of built-in algorithms it provides and the easiness to display graphs and results.

5.1 General procedure

The General Method is a rather straightforward algorithm following the equations described in chapter 2 for the planar approach. In the following subsections, a description for the method, inputs and outputs for the Matlab function and how the user must proceed with it can be found.

5.1.1 Description

The aim of the function is to obtain a first information from the plasma from the I-V curve. Given the assumptions made, a more complex process could be implemented in

order to obtain more precise information about the measured plasma. Four characteristic parameters are obtained, the electron temperature, floating and plasma potentials and plasma density.

First it is searched for the floating potential, the point of the voltage vector corresponding to the lowest of the current points in absolute value. It is good to know this value, or at least its neighbourhood, to get a sense of the plasma performance; even though the value itself is not used for any further calculation, it is useful to limit some ranges for fitting.

The following step is to obtain the plasma potential. The input vectors for the voltage and the current are assumed as smoothed, with a reasonable low noise, $dI < 5\%I$ outside the region of the floating potential, $Vf \pm 3$. The plasma potential coincides with the maximum point of the dI/dV curve. Therefore the gradient is computed directly and plotted. From this first graph, the plasma potential is saved by means of the user interaction with the figure. A proposal for the choice of this value is given in the next section of this chapter.

Next, it is represented the ion saturation range until the floating potential region for a broader point of view. Again, it is needed the action of the user and he must zoom in until the scope focuses on the desired ion range to be fitted.

At this point, two fits are performed on the selected range, a linear fit and constant fit. The first finds the fittest straight line, a first order polynomial, matching the data points. This fit will be used later to correct the current near the floating potential by means of subtracting it and obtaining a pure electron current. Also, an estimation of the saturation current is obtained from the value of this theoretical straight line at the position of the floating potential.

As introduced before, a new vector with the theoretical ion current is constructed. It coincides with the first-order polynomial fit until the current reaches the value of 0. From that point on, all the following values should be replaced by zero; as it is not realistic that ions induce a positive sign current.

This current is subtracted from the data current to obtain the electron current, which should fit an exponential function. To achieve a better range selection, it is plotted the log of this vector. Then, by means of the user interaction with the figure, the most linear range must be decided, bounding it with the plasma and floating potentials, upper and lower limits respectively. Once the user has chosen the range, the data is fitted with a first order polynomial. The temperature is then obtained by 5.1, where a_e is the slope of the straight line fit for the semi-log figure.

$$T_e = \frac{1}{a_e}[eV] \tag{5.1}$$

Once it is found a value for the temperature and the ion saturation current, the density can be obtain form the next relation:

$$n_i = \frac{-I_{sat}}{0.6eS}\sqrt{\frac{m_i}{eT_e}} \tag{5.2}$$

Also, in order to check the behaviour of the sheath, the Debye length is calculated by means of the following expression.

$$\lambda = \sqrt{\frac{\epsilon_0 T_e}{n_i e}} \tag{5.3}$$

5.1.2 Program inputs and outputs

The input is a structure containing the next elements:

- ***'Vdes'*** is the voltage vector from the I-V curve. The units are volts [V].
- ***'I'*** is the current vector corresponding to 'Vdes'. It is recommended that the data set has a length of at least 100 points in order to have a higher resolution when computing the potential magnitudes. The units for the current vector are amps [A].
- ***'lp'*** is the probe length in meters [m].
- ***'lr'*** is the probe radius in meters [m]. The implemented theory assumes a cylindrical probe so modifications in the collecting area must be made if the probe is planar or spherical.
- 'm_i' is the ion mass in kilograms [kg].
- ***'const'*** is a structure containing known constants in the I.S. There are:
  - 'KB': Boltzman constant $[m^2kg/s^2K]$.
  - 'e': electron electric charge [C].
  - 'me': electron mass [kg].
  - 'ep0': vacuum permittivity [F/m].

The output is a structure containing three vectors in the following order:

- ***'res'*** is a 5 element row vector containing the values for the results computed: temperature [eV], plasma density [$m^{-}3$], Debye length [m], plasma potential [V] and floating potential [V].

- ***'err'*** is 4 element row vector containing the errors of the different fits performed by the function. Even though there are only three actual error values involved, it is added a fourth one defined as 'NaN' to comply with the format given by other homologous functions, such as EM, evaluating other theories. The order for the errors is: 'NaN', linear ion fit, constant ion fit and electron fit. All these errors are relative and so they come in percentage (%).

- ***'AuxParam'*** is a 3 element vector whose main objective is to extract auxiliary useful values from the function. For this function, the elements are the limits of the ion range selected, lower and upper, and the slope of the ion straight line fit.

5.1.3 User interaction

The program asks for the action of the user thrice: selection of plasma potential, and choice of ion and electron ranges. The smoothing of the I-V curve strongly affects the easiness to correctly choose the plasma potential. Roughly, it should be selected the maximum point on the dI/dV curve regardless the noise peaks, which can be reduced considerably by smoothing the IV curve previously. This easy way gives a rather good estimation of the plasma potential value. The selection is done by right clicking with the mouse at the desired location of the figure; only the x coordinate is saved.

However, there are some cases where the reliability of the highest peak being the plasma potential is dubious. If the dI/dV curve presents a local maximum before the highest peak, and they are relatively close to each other, the plasma potential to be selected could be either the first peak or the middle point between the two critical points. It is important to follow the same exact procedure for all the analysed cases so as to have a consistent method to apply. For the later analysis in Chapter 6, the first local maximum was the point selected as plasma potential for all the cases.

Regarding the ion saturation range, the aim is to select the straightest line possible below the floating potential. Note that the more extensive is the range considered, the better the extrapolation will result and the more reliable the results for the electron fit will be. The selection of the range is done by zooming in until the figure window encloses all the points desired to fit. Once finished this step, press any key. This procedure also applies to the electron fit range.

The electron saturation range is similar. The point to be avoided is the plasma potential, which is indicated with a red dotted line on the graph. It should be selected a range closer to the floating potential, which is already corrected with the subtraction of the ion current. Even though the floating potential may appear as a limit, it is not, and if the curve to the right of this value is straight enough, it must be considered to be fitted.Also, it is possible that bumps appear close to the floating potential, thus this region should be avoided when selecting the bounds.Note that the possible range to select is going to be much smaller than for the ion case, and so it is more important to fit exactly the most linear segment of the curve and avoid diverging from the real plasma parameters. Again, the selection is done by zooming the desired data range, as for the case of the ion fit.

5.2 EPFL procedure

The next post-processing method was obtained from the university *École Polytechnique Fédérale de Lausanne* and can be found on reference [Furno, 2012]. In contrast to the General procedure, it considers the behaviour of both species for two regions at the same time, the ion saturation range and the electron gain domain. Recalling the equation for the ion saturation current obtained from the Bohm velocity,

$$I_{i,sat} = -e^{-1/2} A_p n e \sqrt{\frac{k_B T_e}{m_i}} \tag{5.4}$$

and the current due to the electron gain,

$$I_e(V_p) = I_{e,sat} exp\left[\frac{-e(V_s - V_p)}{T_e}\right] = \frac{1}{2} A_p n e \sqrt{\frac{2k_B T_e}{\pi m_e}} exp\left[\frac{-e(V_s - V_p)}{k_B T_e}\right] \tag{5.5}$$

$$V_s - V_f = \frac{1}{2}\left[ln\left(\frac{2\pi m_e}{m_i}\right)\right]\frac{k_B T_e}{e} \tag{5.6}$$

Merging the three previous equations together with $I = I_i + I_e$, it is obtained 5.7;

$$I = I_{sat}\left[1 - exp\left(\frac{V - V_f}{T_e}\right)\right] \tag{5.7}$$

However, the effect of the sheath must be often considered, and it is taken into account by the particle α in 5.8. At large negative voltages, the sheath expands and increases the collecting area, implying a higher ion flux. This effect can be observed in the IV in

figure 2.1, as I_{sat} does not saturate.

$$I = I_{sat}\left[1 - \alpha\left(V - V_f\right) - exp\left(\frac{V - V_f}{T_e}\right)\right] \tag{5.8}$$

Once the expression to fit is clear, the problem is choosing the interpolation boundaries. If it is chosen an upper limit higher than the plasma potential, the electron temperature would be overestimated. To find the best upper boundary an interpolation procedure must be performed, called the 'minimum temperature method'. It consist of taking ranges following the expression:

$$min(V) \rightarrow V_f + \Delta V$$

where ΔV goes from 0 to $max(V) - V_f$. From all those ranges, the one that provides the minimum temperature is selected to fit.

5.2.1 Description

As for the case of GM the aim is to obtain a first information from the plasma from the IV curve. Given the assumptions made, a more complex process could be implemented in order to obtain more precise information about the measured plasma. Four characteristic parameters are obtained, the electron temperature, floating and plasma potentials and plasma density.

First it is searched for the floating potential, the point of the voltage vector corresponding to the lowest of the current points in absolute value. It is good to know this value, or at least its neighbourhood, to get a sense of the plasma performance; even though the value itself is not used for any further calculation, it is useful to limit some ranges for fitting.

Next, it is obtained the plasma potential the same way it was done for the GM. The input vectors for the voltage and the current are assumed as smoothed, with a reasonable low noise, $dI < 5\%I$ outside the region of the floating potential, $V_f \pm 3$. The plasma potential coincides with the maximum point of the dI/dV curve. Therefore the gradient is computed directly and plotted. From this first graph, the plasma potential is saved by means of the user interaction with the figure. A proposal for the choice of this value is given in the next section of this chapter.

The following step is to perform the overall fit. It is done, again, by means of the function *fminsearch* applied to an error function between the theoretical current and the actual

current. Once the iteration parameters are obtained, the errors are calculated and displayed.

5.2.2 Program inputs and outputs

The structure for both the inputs and outputs for this procedure is the same as the one for the previous function. It was meant to follow a standard structure and simplify the understanding of the different methods. Despite that effort, the auxiliary variables do change with respect to the GM. The inputs and outputs are detailed below.

The input is a structure containing the next elements:

- ***'Vdes'*** is the voltage vector from the I-V curve. The units are volts [V].
- ***'I'*** is the current vector corresponding to 'Vdes'. It is recommended that the data set has a length of at least 100 points in order to have a higher resolution when computing the potential magnitudes. The units for the current vector are amps [A].
- ***'lp'*** is the probe length in meters [m].
- ***'lr'*** is the probe radius in meters [m]. The implemented theory assumes a cylindrical probe so modifications in the collecting area must be made if the probe is planar or spherical.
- 'm_i' is the ion mass in kilograms [kg].
- ***'const'*** is a structure containing known constants in the I.S. There are:
  - 'KB': Boltzmann constant [m^2kg/s^2K].
  - 'e': electron electric charge [C].
  - 'me': electron mass [kg].
  - 'ep0': vacuum permittivity [F/m].

The output is a structure containing three vectors in the following order:

- ***'res'*** is a 5 element row vector containing the values for the results computed: temperature [eV], plasma density [m^-3], Debye length [m], plasma potential [V] and floating potential [V].

- ***'err'*** is 4 element row vector containing the errors of the different fits performed by the function. Even though there is only one actual error value involved, it is added a set of three more defined as 'NaN' to comply with the format given by other homologous functions, such as GM, evaluating other theories. The error is located at the forth position, being the first three the 'NaNs'. All these errors are relative and so they come in percentage (%).

- ***'AuxParam'*** is a 3 element vector whose main objective is to extract auxiliary useful values from the function. For this function, the elements are the lower limit for the overall fit, the α from 5.1 and the obtained upper limit potential.

5.2.3 User interaction

In contrast to the GM, this function asks for the action of the user only twice; the first for the selection of the plasma potential, and the second for the choice of the lower limit of the overall fit.

Again, the smoothing of the I-V curve strongly affects the easiness to correctly choose the plasma potential. Roughly, it should be selected the maximum point on the dI/dV curve regardless the noise peaks, which can be reduced considerably by smoothing the IV curve previously. This easy way gives a rather good estimation of the plasma potential value. The selection is done by right clicking with the mouse at the desired location of the figure; only the x coordinate is saved.

There are some cases where the reliability of the highest peak being the plasma potential is dubious. If the dI/dV curve presents a local maximum before the highest peak, and they are relatively close to each other, the plasma potential to be selected could be either the first peak or the middle point between the two critical points. It is important to follow the same exact procedure for all the analysed cases so as to have a consistent method to apply. For the later analysis in Chapter 6, the first local maximum was the point selected as plasma potential for all the cases.

Regarding the overall fit, the aim is to select the straightest line possible below the floating potential. Note that the more extensive is the range considered, the better the extrapolation will result and the more reliable the results for the electron fit will be.

5.3 Chen 2001 Algorithm

The following appendix resumes the work done on the third post-processing method, Chen_2001, so as to serve as introduction for future work. The original code was implemeted by Francis Chen in Excel and can be found at [F.F.Chen]. The algorithm procedure is described at [Chen, 2001].

The implemented code consists of four functions: *post_LP_chen2001* , *OPT*, *EstimPlasmParam* and *IonFitERR*. The first is the main script of the code, in which the rough estimations for the variables of interest is done and where the optimization function is called. It follows the same name structure as the other functions to simplify its use. *OPT* is the function being optimized, whose main output is the error of the procedure. *EstimPlasmParam* and *IonFitERR* are sub-functions and were created to simplify visually the procedure. They contain all the mathematical operations giving the parameters.

The algorithm is the following. First, a initial guess for each of the four variables is calculated. According to the original algorithm, these four parameters are the electron temperature T_e, plasma density n and plasma potentials for each of the species, ions and electrons, $V_{s,i}$ and $V_{s,e}$ respectively.

In order to estimate the space potential, it must be computed dI/dV, as for the cases of GM and EM. Even though the data must be smoothed before computing this ratio, dI/dV results in a very noisy curve. The voltage for the maximum of the ratio can be considered to be the space potential V_s. The surroundings of the maximum could be again smoothed to obtain a better approximation but it is not really necessary as this is just an estimation and the difference is not going to be larger than a 5%. The value found will be the initial guess for both plasma potentials.

Regarding the temperature, an approximate value is obtained from the ratio between the current I and dI/dV at the space potential V_s previously obtained. This ratio results directly on the electron temperature in electron volts. For this estimation it is actually recommended to smooth the critical point surroundings as a small difference in V_s would lead to a totally different value of the temperature.

For the plasma density, the Bohm criterion is used. The plasma is assumed to be quasi-neutral so the estimation of the ion density is valid for the whole plasma.

Once the four estimations are done the Matlab function *fminsearch* is used to find the minimum of *OPT*. Inside it, the sub-function *EstimPlasmParam* is called, giving new values to the four variables of interest by working with the I-V curve and the previous estimations. Together with the results of the plasma parameters, it is also extracted the

errors for the fits performed. These are joined into a figure of merit which is optimized by means of the *OPT* function. It was also tried to monitor the differences in the parameters between following steps in order to find convergence but the approach had more issues so it was discarded.

With respect to the function EstimPlasmParam, two different fits are done, an ion fit and an electron fit, a similar procedure to the GM but with the interesting fact of being automatic.

The ion fit is done by means of the function *IonFitERR* in which the only parameters optimized are the ion plasma potential and the plasma density. First, it is calculated the Debye length and χ, a parameter indicating how large is the probe compared to the plasma region it interferes. According to that constant, Chen provides a table of coefficients, the derivations of these can be found on [Chen, 2001], for a function defining the theoretical ion current for the input plasma parameters. From the difference between this theoretical current and the measured an error magnitude is given as output of *IonFitERR*. This process is repeated until the smallest error is found using the Matlab predefined function *fminsearch*. Note that even though the temperature is not modified during this process, it is indeed used as constant.

Once the ion current is calculated for the pair of values of n and V_{si}, the electron current is the result from adding up the total and the negative ion current, $I_e = I + I_i$. The electron fit is then performed using the equation 2.9 for electrons. Again, the minimum error is found this time varying the temperature and the electron plasma potential, T_e and V_{se}.

The errors of both fits are extracted from *EstimPlasmParam* as outputs in order to follow an iterative procedure until the smallest error for both operations is found.

Unlike GM and EM, this algorithm is more time consuming but it is fully automatic. The issue appears when the convergence is not easy to achieve. If the set of initial guesses is relatively different from the real values, and due to the fact that the fits are not performed exactly in the same operation, if the results from the first sub-function diverge to other local minimum different from the real set, the second function operates already on the wrong direction.

Furthermore, it is already warned by Francis Chen in his paper [Chen, 2001] that the convergence of this algorithm relies on a quite accurate estimation of the four parameters.

In addition, a suspected reason for the fail of the algorithm is the use of two different plasma potentials for ions and electrons. It is left for future work to investigate this issue.

Chapter 6

Results and Comparisons

The Helicon plasma thruster performance, closely related to the temperature and density of the plasma, is governed by the following parameters:

- Geometry configuration
- Mass flow rate
- Gas type
- Radio frequency power
- Magnetic field distribution

During the experiments three of the operation parameters were changed. These three are the mass flow rate, the radio frequency power and the geometry configuration.

It must be pointed out that a large amount of data was analysed, above 150 IV curves, with the implemented methods but only the most representative ones were chosen to be displayed. The aim of the given figures is to show the interpretation of the processed data.

6.1 Results description

The main aim of this section is to show the outputs of the processing codes, General and EPFL methods, for a sample IV curve and comment briefly on them. The processing algorithm Chen2001 was not considered due to wrong convergence of the method.

6.1.1 General code

The results displayed for the GM are from K_A1_112808, data curve obtained on July 22nd from the home helicon plasma thruster.

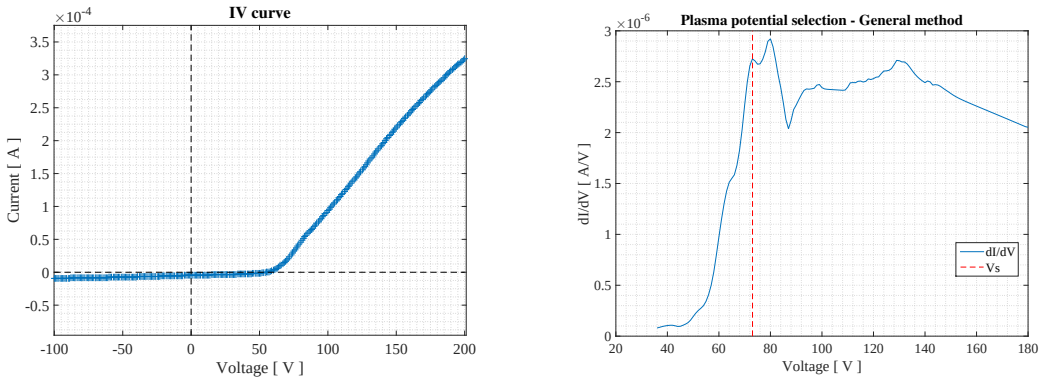

(A) IV curve (B) Plasma potential selection

FIGURE 6.1: General Method output

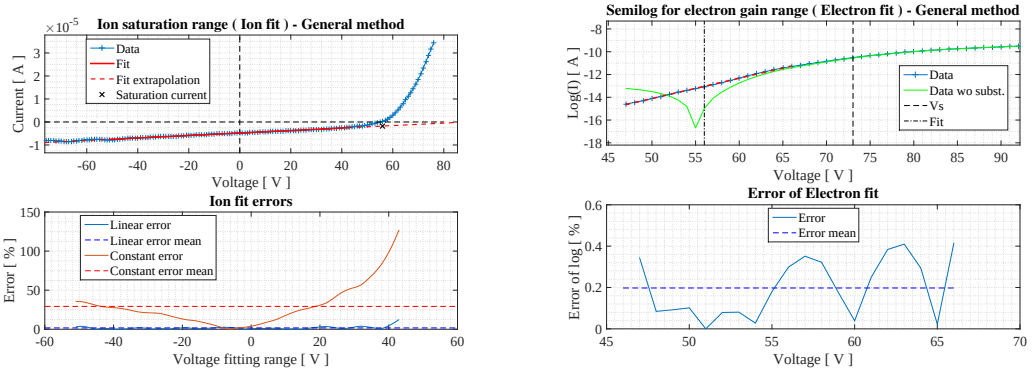

(A) Ion fit (B) Electron fit

FIGURE 6.2: Fits for General Method, K_A1_112808

As explained in the code implementation section, three graphs are the output from the General Method code, together with the values of the four plasma parameters. It is also plotted the IV curve.

The plasma potential selection , figure 6.1b, simply plots the calculated gradient dI/dV versus V in blue. After the selection of V_s, a red dotted vertical line is displayed at such value.

In figure 6.2a, at the left, the ion fit is presented. The fit itself, the linear fit, is shown in solid red line, bounded by the selected region, whose choice was done looking for the most linear interval in the negative current regime. In addition, the line expression is expanded, red dotted shape, for all the potential. Below the floating potential, the

corresponding point of the linear fit is marked with a black cross indicating the ion saturation current, I_{sat}.

At the right panel, the electron fit is exhibited. It is plotted the logarithm of the current versus the potential of the probe. The fit consist of achieving the most linear region before the plasma potential. The fit performed is shown in a red dashed line. The value of the floating potential and the plasma potential are given as a reference.

After taking a look to the graphs, it is noticed that the IV curve is not following the theory. Usually it would be expected to have the electron saturation point not as far away from the floating potential as the presented case. This behaviour is also related with the DI/DV graph, where there is not a clean maximum but a plateau. Furthermore, it was assumed that the knee in IV indicated the plasma potential, but it is only true when the plasma is non-drifting [Hutchinson, 2002]. Some external effects, such as the magnetic fields of the helicon and the RF plasma could modify the IV curve, and so, the plasma potential determination [Sudit and Chen, 1994].

Regarding the fits performed, both curves are accompanied by the error distribution associated. The errors shown are relative, expressed in % of the real value of the current. It is seen for the ion range the divergence between data and fit for the region of the floating potential. This is due to the electron current, that is not considered but it begins to become important as the probe potential increases.

Finally the results obtained from the process of this IV curve are the following.

K_A1_112808			
Electron temperature [eV]	Plasma density [m^{-3}]	Plasma potential [V]	Floating potential[V]
5.8028	2.572×10^{15}	66.3	56

TABLE 6.1: Plasma parameters for K_A1_112808

6.1.2 EPFL code

The results displayed for the EM are from K1_A1_173409, data curve obtained on June 27th from the home helicon plasma thruster.

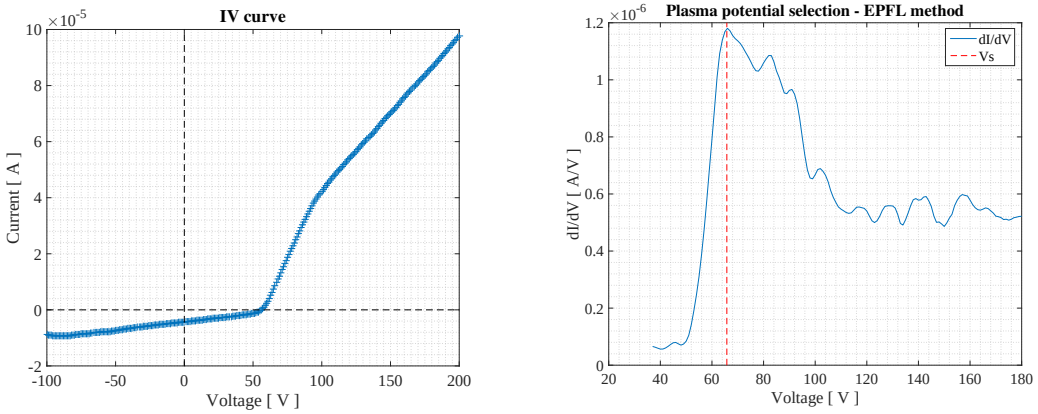

(A) IV curve (B) Plasma potential selection

FIGURE 6.3: EPFL Method output, K1_A1_173409

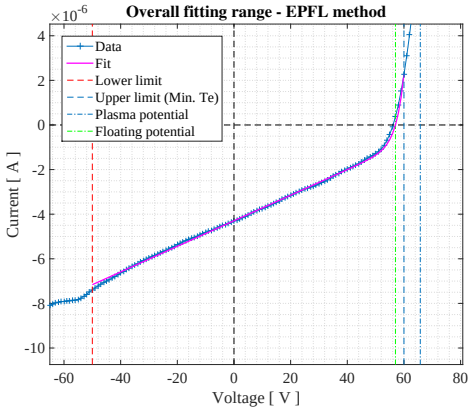

FIGURE 6.4: Overall fit for EPFL Method, K1_A1_173409

For the case of the EPFL Method, only one fit is performed so essentially two graphs are the output of the function, the V_s selection and the fit itself.

The plasma potential selection, on the left of figure 6.3, follows the previously said about the figure 6.1b, General Method case. The chosen value for V_s is indicated with a red dashed vertical line and corresponds to the point selected by the user.

For the case of the overall fit graph, figure 6.4, the fit is drawn in a solid magenta line over the data points. Also, four reference vertical lines are included for additional information. Two of them are the fit bounds, both consisting of dashed lines. The lower limit, in red is selected by the user and the upper, in light blue, is calculated by the minimum temperature method, described in chapter 5 and can be found on the EPFL method reference. The two remaining additional lines are located at the values of the plasma potential and floating potential, blue dotted-dashed and green dashed lines respectively.

To obtain a good fit, the electron range must be short. An important external effect affecting this IV curve is the radio-frequency influence, which flattens exponential electron region. This strongly affects the way the IV curve must be processed as a shorter interval must be considered to obtain the electron behaviour, that is capture the exponential effect. Focusing on the lower knee neighbourhood the fit for the electron exponential is valid enough and the effect of some real complex phenomena is avoided.

It could happen that the fact of considering all the range from the lower V_s to the end of the knee contributes to a higher mean error due to the including of the V_f surroundings. It will be pointed out for later curves in the next chapter.

So then, the results obtained from the process of this IV curve are the following.

K1_A1_173409			
Electron temperature [eV]	Plasma density [mˆ-3]	Plasma potential [V]	Floating potential[V]
2.7053	2.1×10^{15}	65.9	57

TABLE 6.2: Plasma parameters for K1_A1_173409

6.2 Comparison procedure

This section concerns the difference between both implemented methods. First it is shown the procedure followed to contrast the outputs and then an analysis is brought about the performance of each method for different conditions, such as high or low temperature and high or low density.

6.2.1 Procedure

As for the case of the post-processing procedures, the comparison between both methods was done by a function implemented in the software [Mathworks]. Briefly, the function extracts the plasma parameters from each of the procedures and calculates the theoretical IV curves associated to those sets of values. The final results can be seen further in this section.

The theoretical curve used to validate the results is defined as in the document [Furno, 2012] on page 37.

$$I = I_{sat}\left[1 - \alpha(V - V_f) - exp\left(\frac{V - V_f}{T_e}\right)\right] \tag{6.1}$$

In 6.1 the unknowns calculated when performing the fit are I_{sat}, α and T_e.

A more in detail procedure of the comparison script is given below.

The functions *'postp_LP_General'* and *'postp_LP_EPFL'* are called and the plasma parameters of each saved. It must be tried to select the same common points for both functions, such as the lower fitting limit or the plasma potential.

The saturation current is calculated, given by the equation 2.9, that is doing the reverse process to the one done inside the function basically.

Regarding the bounds for the function range, they are derived from limits from both functions. For the upper bound, it is selected the upper limit for the overall fit of the EPFL method. This position was calculated with the minimum temperature method from citeEPFL and states the point at which the IV curve diverges from the theoretical expression and begins to suffer the real effects of the probes. For the lower bound, it is calculated the mean between the lower limit for the ion fitting range of the GM and the lower limit of the overall fit of the EM. These two values should be very similar, as the criterion to select them should have been the same, exclude weird behavior of the current for very negative voltages.

Once the limits are clear, the ranges are calculated and the function evaluated with the relevant parameters: I_{sat},T_e and α, for each case. These are values are obtained or derived from the function outputs.

Finally, for a more quantitative comparison between the methods, the error with respect to the original IV curve is calculated. It is done the same way as on the other functions, shown by 6.2, and expressed as relative errors.

$$\delta I = \left| \frac{I - I_x}{I} \right| \times 100 \tag{6.2}$$

where I is the original current vector and I_x is the theoretical current vector for method X.

6.2.2 Results

Among all the IV curves analysed, five that were of special interest to compare the methods are specified in the Table 6.3. It was selected the most different conditions present, lowest and highest temperatures and densities, out of the whole group of data acquired in the lab. The four selected sets were obtained from the HPT at the end of June and July, and it can be noticed how the order of acquisition affected the parameters.

			Helicon thruster conditions		
	Probe	Condition	mfr [sccm]	Magnetic field [G]	Internal distance
Random bata 3	X	Ideal	-	-	-
K1_C1_131228	C	Low n	20	300	short
K1_B1_131107	B	Low T_e	15	600	mid
K1_C2_171810	C	High n	x	x	x
K_C2_113028	C	High T_e	x	x	x

TABLE 6.3: Thruster conditions for data to compare

This pattern will later be explained at the end of the results section. It is also shown a quasi-ideal curve.

The dimensions of the probes refered in Table 6.3 can be found on Table 4.1 in Chapter 4.

6.2.2.1 General condition

First it is going to be analysed an ideal IV curve as general case to check the performance of the methods. This specific curve was not data taken from experiments performed in this university, but was provided by the project advisor. There is a considerable difference between the plasma of this experiment and the one of the home helicon thruster.The results obtained from both functions are displayed in the Table 6.4.

RandomData_3				
Plasma parameters	Electron temperature [eV]	Plasma density [m^{-3}]	Plasma potential [V]	Floating potential [V]
General Method	5.3313	4.352×10^{17}	31.5	26.6
EPFL Method	5.6862	4.391×10^{17}	31.5	

TABLE 6.4: Plasma parameters for RandomData_3

Next it is shown the different fits together with the comparison of both theoretical curve and the errors associated.

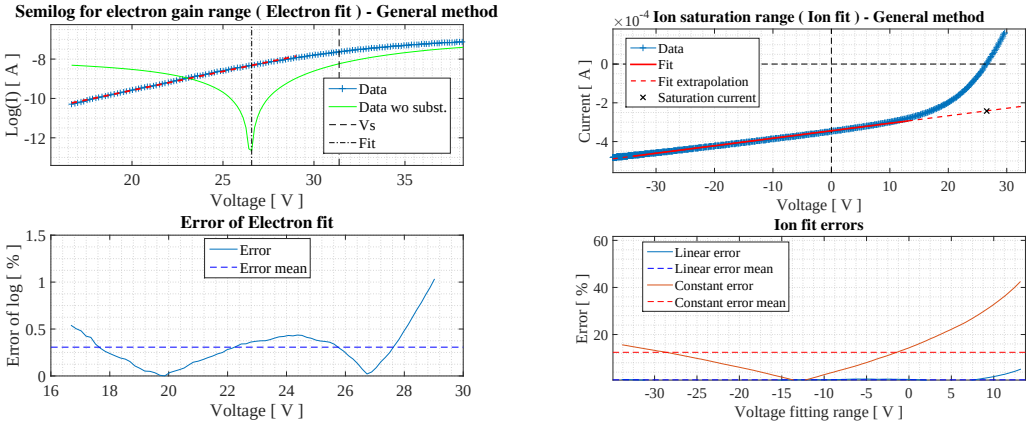

(A) Ion fit (B) Electron fit

FIGURE 6.5: General method output, RandomData_3

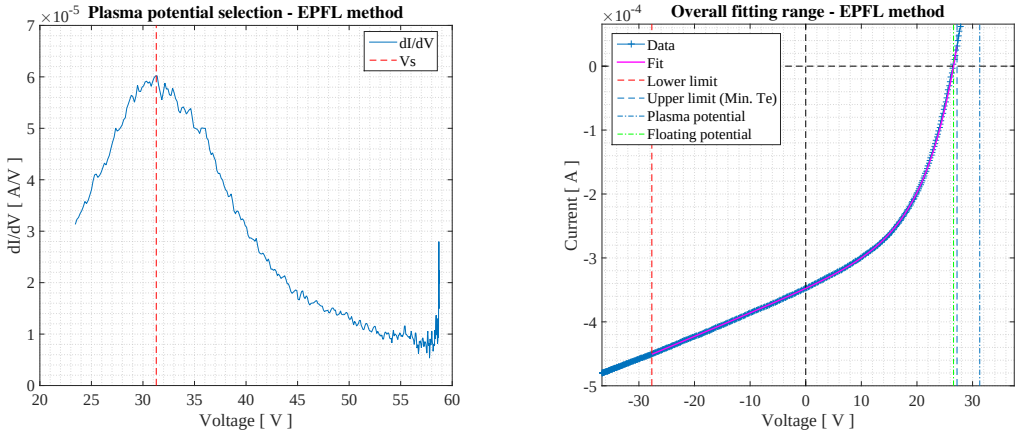

(A) Plasma potential selection (B) Overall fit

FIGURE 6.6: EPFL method output, RandomData_3

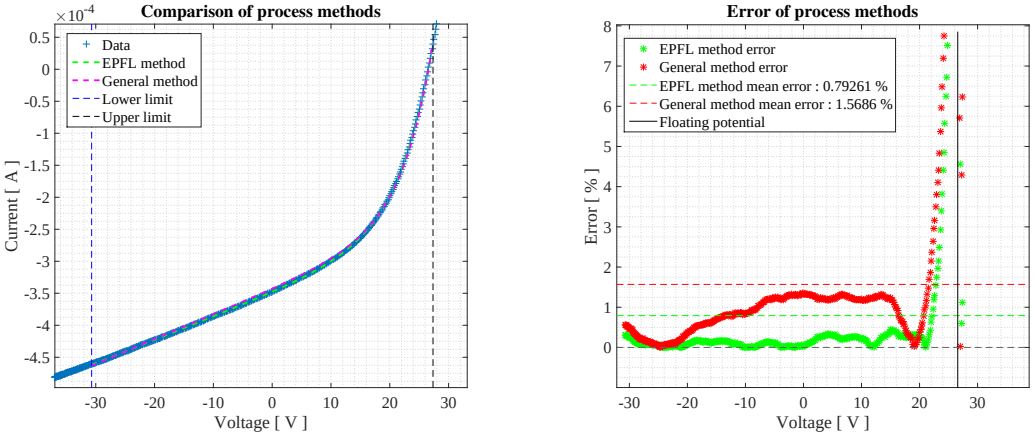

(A) Methods comparison (B) Comparison error

FIGURE 6.7: Compare function output, RandomData_3

Even though the actual difference between the methods can be observed on the last two graphs,the other four show how the methods were carried out.

Regarding the most significant figure, the error graph, it shows the general trend for the error distribution. For negative potentials, the error is low, normally $< 5\%$, and it increases when approaching the floating potential. The ion range usually concerns a very robust straight line easy to fit, low noise, and the floating potential neighbourhood contains points whose value is very close to zero. Recalling 6.2, the curve noise divided by these small numbers give the apparent high error.

About the data, there is a significant difference between the error of the methods along the ion range. The General Method, shown in red, seems to be neglecting an important contribution to the current, and that is precisely the reason for the discrepancy. The GM fits the ion range straight line and then subtracts the ion current to the total current and fits the log(I). Therefore, the electron current is not considered when fitting the ion range, and , as it can be noticed, it is particularly important for almost the entire range. In contrast, EM ,green curve, does account both currents, ion and electron, on both ranges as a single fit is applied with 6.1, where both contributions are considered.

6.2.2.2 Low density

Among the data analysed, one of the sets resulting in the lowest densities was taken the June 23rd at 13h 12m 28s with probe C. The results obtained from both functions are displayed in the Table 6.5.

K1_C1_131228				
Plasma parameters	Electron temperature [eV]	Plasma density [m^{-3}]	Plasma potential [V]	Floating potential [V]
General Method	4.8973	1.188×10^{14}	57.9	37
EPFL Method	4.7142	9.579×10^{13}	57.9	

TABLE 6.5: Plasma parameters for K1_C1_131228

Next it is shown the different fits together with the comparison of both theoretical curve and the errors associated.

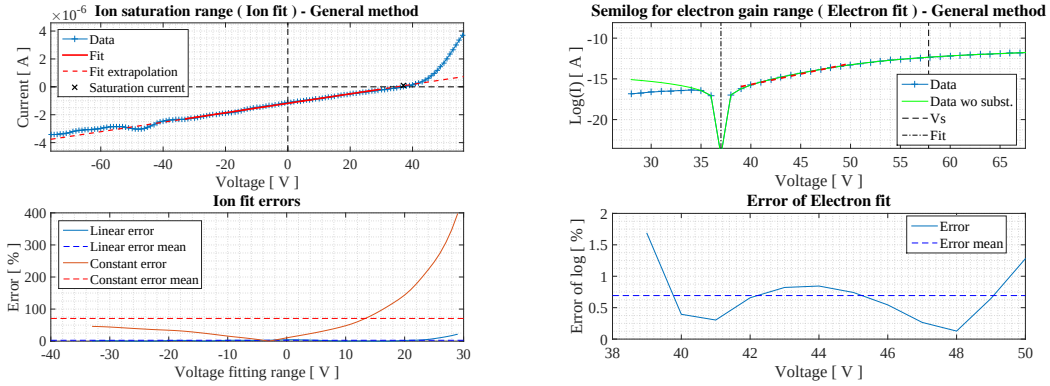

(A) Ion fit (B) Electron fit

FIGURE 6.8: General method output, K1_C1_131228

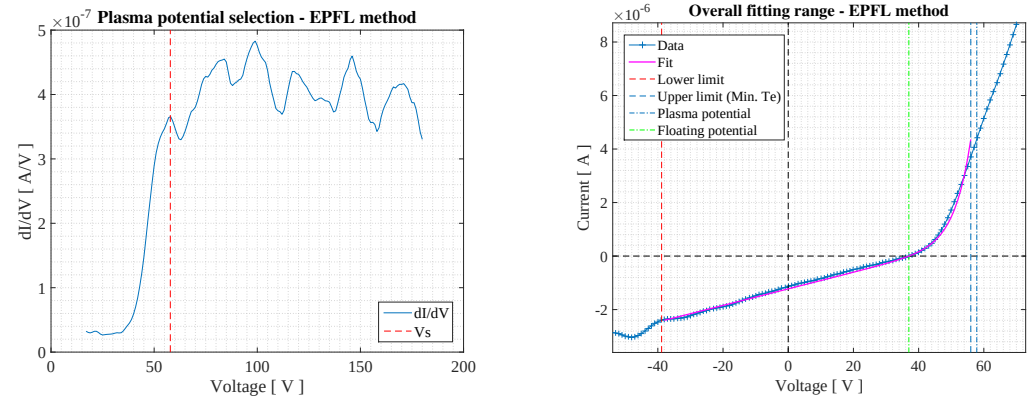

(A) Plasma potential selection (B) Overall fit

FIGURE 6.9: EPFL method output, K1_C1_131228

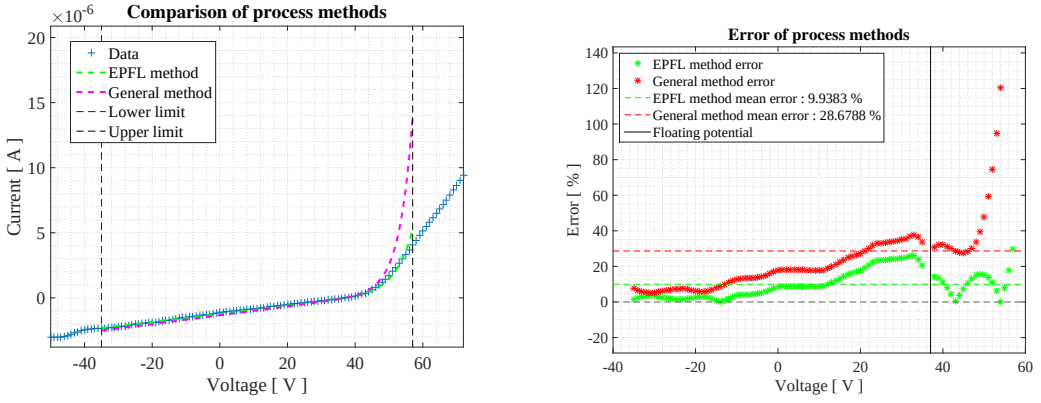

(A) Methods comparison (B) Comparison error

FIGURE 6.10: Compare function output, K1_C1_131228

First, it must be pointed out the disparity between this case and the previous. The ion range presents some bumpy region that reduces the effective interval, the electron fit for GM shows an anomaly on the electron current and the plasma potential selection is confusing. All these issues appear due to the low density of the plasma, where the ion

and the electron current are small. Then, at V_f, due to the electron current being so weak, the exponential is not yet observed and the ion current linear behaviour dominates. This implies that the ion saturation current taken is positive, and when subtracting it to the total current, a discontinuity appears at the electron fit graph. In addition, at low densities the plasma is more prone to be unstable, which may be the reason for the bumpy region in the ion fit.

Regarding the methods performance, the trend is the same; GM error is larger at the ion range for not considering the electron current in the ion fit. Despite that fact, the order of magnitude of the error for both methods is larger than that for the ideal curve.

6.2.2.3 Low temperature

Among the data analysed, one of the sets resulting in the lowest temperature was taken the June 28th at 13h 11m 07s with probe B. The results obtained from both functions are displayed in the Table 6.6.

K1_B1_131107				
Plasma parameters	Electron temperature [eV]	Plasma density [m^{-3}]	Plasma potential [V]	Floating potential [V]
General Method	2.6232	1.746×10^{15}	68.1	48
EPFL Method	2.5893	1.778×10^{15}	68.1	

TABLE 6.6: Plasma parameters for K1_B1_131107

Next it is shown the different fits together with the comparison of both theoretical curve and the errors associated.

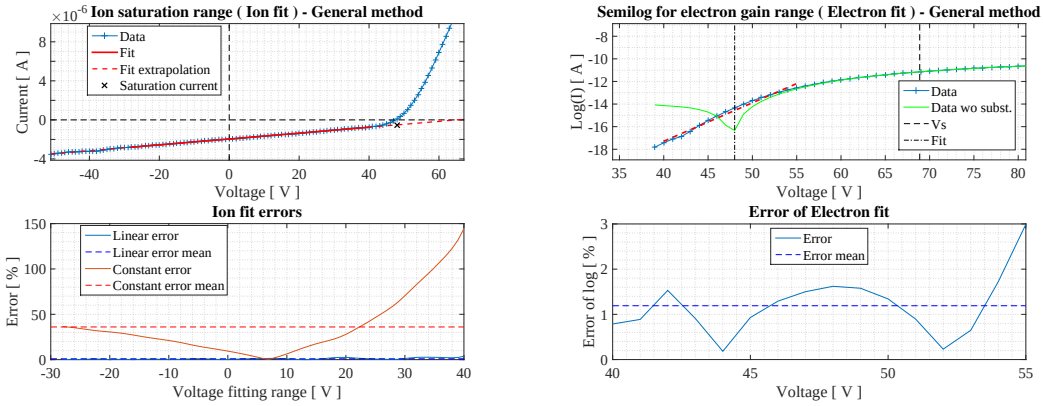

(A) Ion fit

(B) Electron fit

FIGURE 6.11: General method output, K1_B1_131107

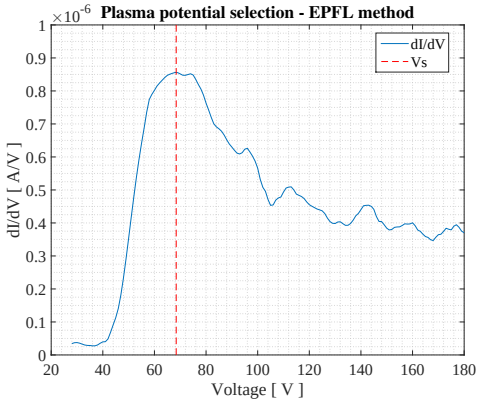

(A) Plasma potential selection

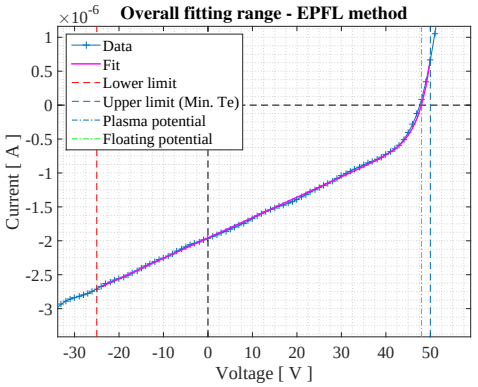

(B) Overall fit

FIGURE 6.12: EPFL method output, K1_B1_131107

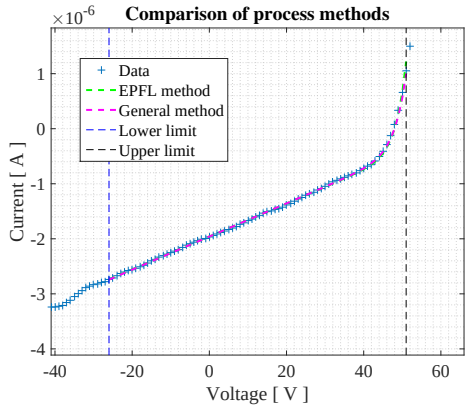

(A) Methods comparison

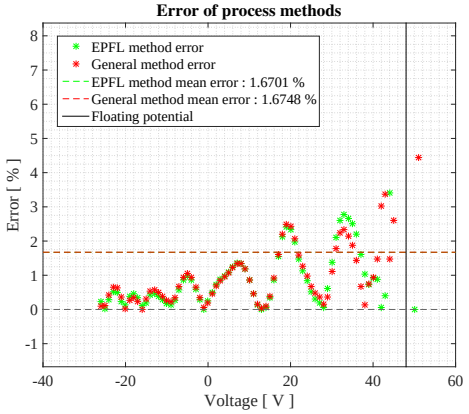

(B) Comparison error

FIGURE 6.13: Compare function output, K1_B1_131107

Now, the electron fit from GM has improved, a linear region can be easily identified, but the ion range has more bumps than the last case; making it noticeable on the error graph. On the other hand, the selection of the plasma potential was clear.

In contrast to previous curves, GM achieves a lower error than the EM despite ignoring the electron current. The main reason for this is the temperature. The exponential of the electron current depends directly on the temperature, and the low temperature of this case makes the electron current negligible below the floating potential. Furthermore, the effect of the temperature can be noticed by looking at the reference position of the the floating potential with respect to the lower knee. If V_f is above the knee, it means the electron current does not overcome that of the ions until the exponential is well developed, and so it implies that the temperature is low.

6.2.2.4 High density

Among the data analysed, one of the sets resulting in the highest densities was taken the June 30th at 17h 18m 10s with probe C. The results obtained from both functions are displayed in the Table 6.7.

K1_C2_171810				
Plasma parameters	Electron temperature [eV]	Plasma density [m^{-3}]	Plasma potential [V]	Floating potential [V]
General Method	4.4592	6.735×10^{15}	55.5	48
EPFL Method	3.8791	7.134×10^{15}	55.9	

TABLE 6.7: Plasma parameters for K1_C2_171810

Next it is shown the different fits together with the comparison of both theoretical curve and the errors associated.

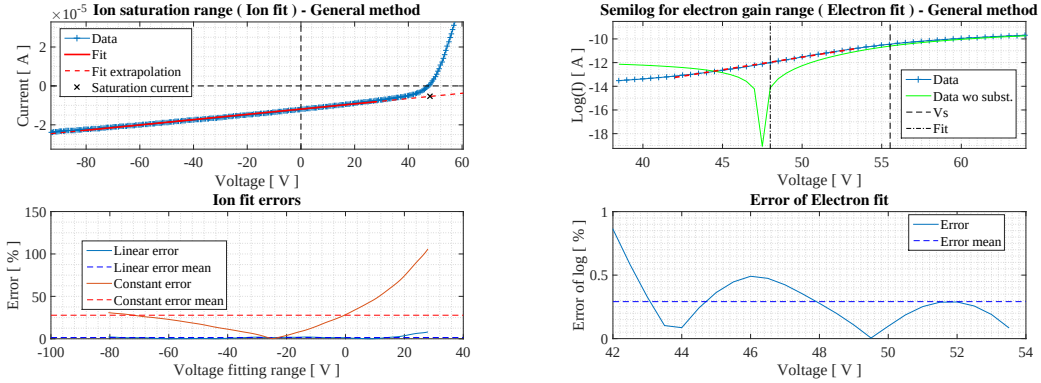

(A) Ion fit (B) Electron fit

FIGURE 6.14: General method output, K1_C2_171810

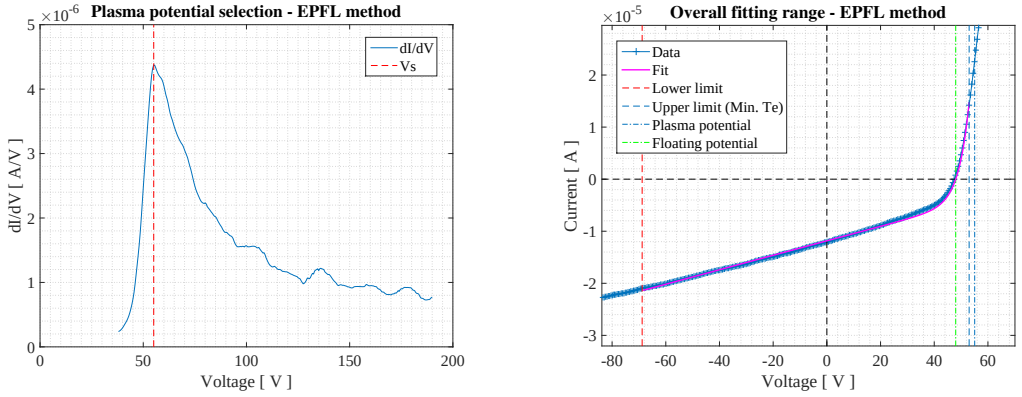

(A) Plasma potential selection (B) Overall fit

FIGURE 6.15: EPFL method output, K1_C2_171810

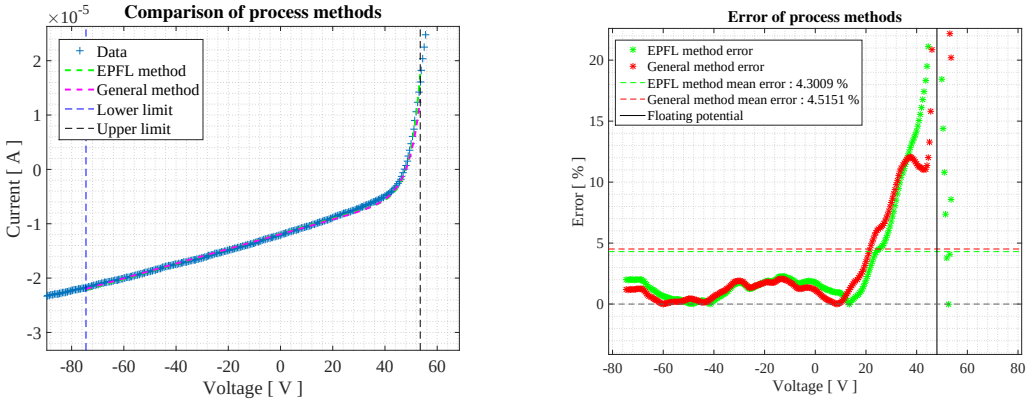

(A) Methods comparison (B) Comparison error

FIGURE 6.16: Compare function output, K1_C2_171810

For the high density curve, the data improved the reliability; there is a clear selection of plasma potential and the linear fits ranges, both ion and electron, are long enough. Also, the electron exponential can be easily seen.

Now, considering the errors, both methods present almost the same mean error. There are no significant differences in the distribution except foe the neighbourhood of the floating potential, where GM approximates closer to the curve than EM. This case is similar to the low temperature case, as the neglecting of the electron current in the ion range fit does not imply a higher error.

6.2.2.5 High temperature

Among all the data taken in the laboratory, only the last sets obtained, measured in July, present a high temperature enough. This fact is closely related to the modifications of the thruster performed the first weeks of July. An important change made on the helicon is the antenna configuration; the helical antenna of the thruster was replaced by a double loop one. Also, the radio frequency power system was improved. As it will be seen later, these modification increased both the density and the temperature of the plasma.

The next evaluated curve was taken on July 22nd at 11h 30m 28s. The plasma parameters obtained are arranged below.

Next it is shown the different fits together with the comparison of both theoretical curve and the errors associated.

Despite the fact this set yields the best plasma of the analysed group, as parameters approach the nominal ones for the thruster, the selection of the plasma potential is yet

K_C2_113028				
Plasma parameters	Electron temperature [eV]	Plasma density [m^{-3}]	Plasma potential [V]	Floating potential [V]
General Method	8.2177	1.341×10^{16}	40.4	34
EPFL Method	7.8452	1.393×10^{16}	40	

TABLE 6.8: Plasma parameters for K_C2_113028

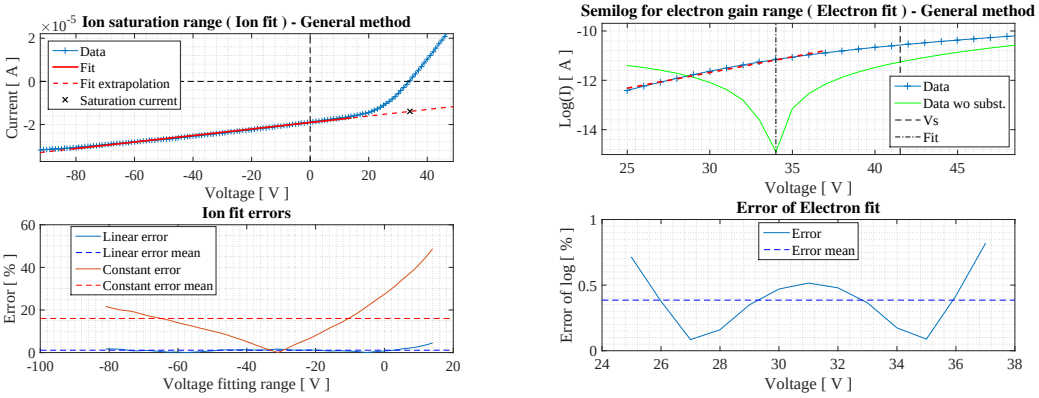

(A) Ion fit (B) Electron fit

FIGURE 6.17: General method output, K_C2_113028

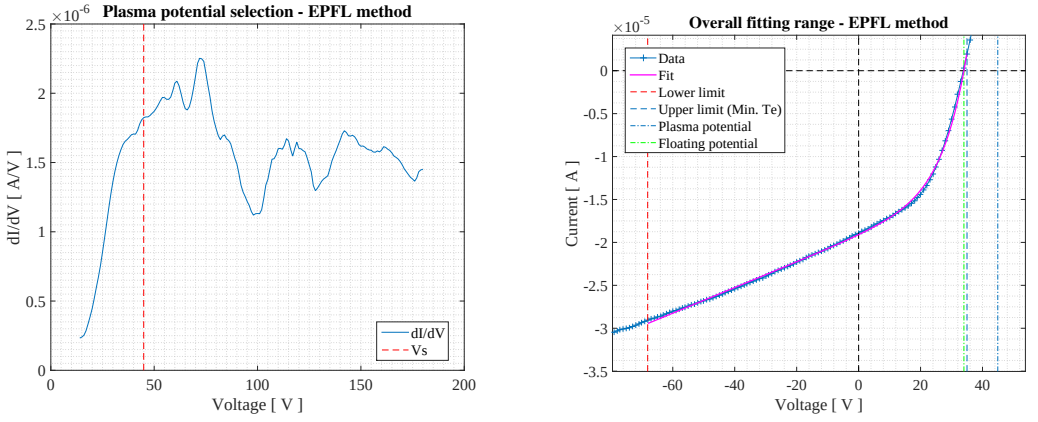

(A) Plasma potential selection (B) Overall fit

FIGURE 6.18: EPFL method output, K_C2_113028

confusing. It was selecting that point following the intuition; the plasma potential is usually right after the steep climb, that is, the first local maximum(global if the curve is quasi-ideal). All the following oscillations is the smoothed noise that makes difficult to correctly select the potential.

The behaviour of the methods is again partially expected; the error is higher in the GM than in the EM for a zone of the ion region. However, there is a 10 V interval around $V = 0$ for which the GM error is very small compared to the EM. It must be

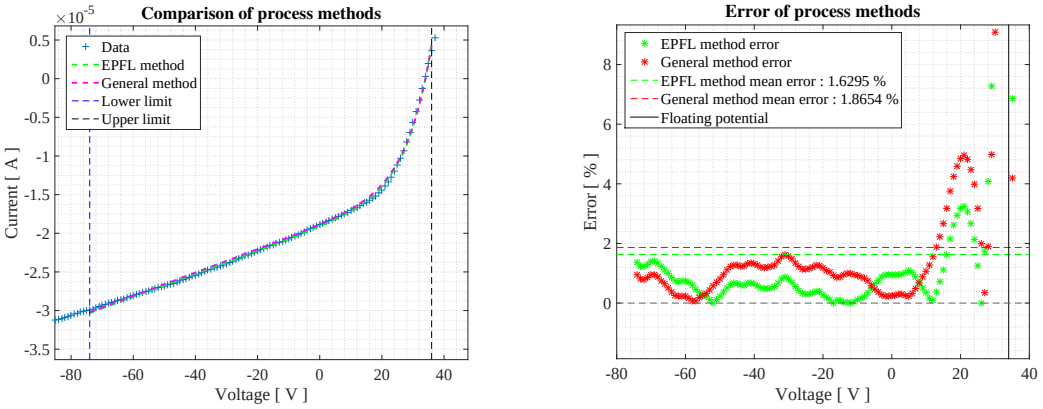

(A) Methods comparison (B) Comparison error

FIGURE 6.19: Compare function output, K_C2_113028

kept in mind that the EM fits the overall curve, this is, searches for the minimum total error, being disadvantaged in certain zones. Then, this fact proves that the GM can give locally better fits, in particular for the ion linear region. In addition, the advantage of GM is that the floating potential region is completely discarded; the theoretical curve associated to it is constructed with the information extracted from the selected ion range and the electron log graph fit alone.

Chapter 7

Regulatory and Socio-economic Framework

7.1 Regulatory framework

Regarding the task of this project, currently there are no regulations applying to the manufacturing of any kind of plasma diagnostics probe or to the data processing of the IV characteristics.

However, as an experimental project, there is a regulation set concerning the occupational risk prevention during the laboratory activity. Given the experiment performed and the facilities used, the following national Spanish laws must be considered:

- Law 31/1995, November 8th, about occupational risks and safety.
- R.D. 29/1997, January 17th, rules about prevention services.
- R.D 299/2016, July 22nd, about health protection and labour safety from electromagnetic fields exposure.

Also, the University Carlos III de Madrid posses internal regulations concerning its employees occupational health and safety measures. For the correct proceedings of such rules, it is provided a safety handbook, which can be found on the next website, `http://portal.uc3m.es/portal/page/portal/laboratorios/prevencion_riesgos_laborales/manual`. This manual contains important points regarding the topic of this thesis, such as, general laboratory facilities risks, electrical risks and compressed gases manipulation risks.

7.2 Socio-economic impact

The world, the society, is increasingly worried about the use of non-renewable resources to produce energy and the possibility of lacking them in a near future. More and more companies and governments are raising awareness of the advantages these resources have and many of the industrial development is aiming that direction.

However, the actual revolution is the controlled nuclear fusion. The concept is based in producing a self-stable reaction in which atomic nuclei fuse together and release energy. This energy can afterwards be extracted and used. However, this reaction needs a particular environment and it is achieved in a magnetic confinement device such as the tokamak.

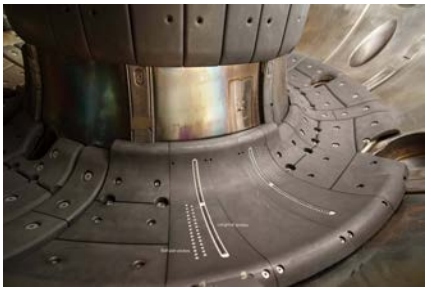

FIGURE 7.1: Langmuir probes array on the COMPASS Tokamak, `http://www.ipp.cas.cz/sd/novinky/hlavni-stranka/160913_divertor.html`

For the development of this thyroidal chambers, plasma diagnostics play a key role, as the plasma confinement is a critical operation and even more if it is totally controlled. One of the most indispensable tools are the Langmuir probes, which the plasma parameters can be monitored with during its operation.

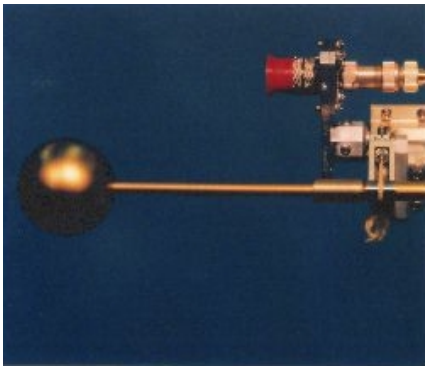

FIGURE 7.2: Swedish Institute of Space Physics Langmuir probe on Cassini mission to Saturn, `http://www.space.irfu.se/cassini/`

Other important issue closely related to the Langmuir probe and to plasma diagnostics in general is the "Space Race". Humanity has been expanding its control limits since it first appeared, and now it is the turn of our solar system. For that, the use of new technologies for the space propulsion is required. Electric and magnetic propulsion has been discovered to have great potential in this environment, and so, more and more resources are being spent on this technology.

However, in order to correctly develop the plasma thrusters taking us to the stars, a robust and reliable measuring system is needed to monitor the evolution of these devices and steer the efforts in the right direction. One of the most useful plasma diagnostics system is the Langmuir probe, for its low manufacturing price, its easiness to install in the laboratory and the straightforward the results are analysed. It is considered a fundamental item in any plasma laboratory and, in contrast to other diagnostics methods, it can even be operated in space. This implies a great advantage over any other device as it can be

installed in the spacecraft and check in-operation the plasma state or how the thruster is reacting to any condition that may arise.

Having explored a global perspective of the current context of the Langmuir probes, it is understood the interest to study these diagnostics devices and develop processing codes. The advances in IV characteristics processing pulls these objectives closer. In particular, one of the main applications of this project has been, and still is, to follow the Helicon Thruster development of the EP2 team and check how the modifications done on the device affect the plasma emitted.

7.3 Project budget

The following section shows the budget associated to this project, which is split into three different parts.

- Manufacturing Cost
  This group considers the materials used for the fabrication of the probes as well as the labour needed for the manufacturing. The unit cost of the probes accounts for the tungsten, the alumina protection, the BNC connector and the kapton cable between others.

Item	Quantity	Unit Cost	Total Cost [€]
Probe materials	5 probes	30 €/probe	150
Labour	20 h	15 €/h	300

TABLE 7.1: Fabrication costs

- Experiment Cost
  The budget associated with the costs of performing the experiment is considered in this point. It includes the time the vacuum chamber has been doing vacuum and the thruster working for acquiring the data. Inside that item it is also considered the rented electronics [KEITHLEY] to correctly save the IV curves. The unit cost of the renting time is expressed in days so the hours of measurements are displayed on that same time scale. The actual number of days performing measurements was much higher.

Item	Quantity	Unit Cost	Total Cost [€]
Chamber & Equipment rent	3 days	400 €/day	1200

TABLE 7.2: Experiment costs

- Processing and Analysis Cost

  It is considered the necessary equipment to carry out the post-processing functions implementation and analysis of the results, together with the software license and the engineering hours devoted.

Item	Quantity	Unit Cost	Total Cost [€]
Computer	1	500	500
Matlab License	1	500	500
Engineer hours	550	19	10450

TABLE 7.3: Processing and analysis costs

The total budget is resumed in the next table.

Item	Cost [€]
Manufacturing Cost	450
Experiment Cost	1200
Analysis Cost	11450
Total Cost	13100

TABLE 7.4: Total cost of the project

Chapter 8

Conclusions

Langmuir probes are by now an antique way of extracting information from the plasma, but yet a largely used diagnostics device. The fabrication process is cheap and simple compared to other probes and the results obtained, processed in a fast way, are valid enough to give a broad idea about the measured plasma.

In addition, it is still reliable in our days regardless the complexity added with the new plasma emitters, involving magnetic fields from thrusters nozzles and new plasma plumes structures yet to fully understand, compared to the glow discharge for which the probes were designed.

The assumptions made throughout the work were acceptable, given the results on Chapters 7 and 8, avoiding the complex physics of real effects as secondary electron emission, effect of magnetic fields and many other contributions that it is known plasma is affected by.

Regarding the performance of the methods, the EPFl method is concluded to be more robust than the General Method for its consideration of the electron current below the floating potential region. It is also suitable to perform the processing of large amounts of data sets as it is faster than GM and easier to use. The most challenging step of the General Method is the selection of the electron fit in the semi-log scale.

Also, it is true that the General method is too dependent on the interaction of the user. Moreover, the number of possible different situations is so high that, first, it is difficult to decide a general criterion to select the ranges of every curve, and second, it may be confusing to follow rigorously that criterion in some special cases as the acquisition of data may be inaccurate.

However, this does not imply that the General method should be totally discarded. When performing the fits, it is clearly understood how the currents are behaving and

where can be the problem existing, if any. Furthermore, it can be used as a second check process in case EM is suspected to fail.

It must be pointed out the evolution of the quality of the plasma analysed. It was not possible to correlate the plasma parameters obtained from the IV curves to the helicon thruster conditions creating such plasma, mainly because the plasma is not stable enough and yet there are a relative high number of unknowns concerning the thruster operation itself. So although changes have been observed according to different thruster configurations, the relation between the plasma parameters T_e and n and the factors still need further studies.

Nonetheless, some information can be actually extracted about the thruster when checking the acquisition dates in chapter 8. The plasma have been acquiring a higher density each time it was fired improving the performance of the methods. To sum up, this work have served as checking stimulus of the development status of the thruster.

8.1 Future work

Even though the project is completed successfully, there is work that can be done to follow the direction of this thesis.

It may be very useful to manufacture a versatile Langmuir probe capable of being modified inside the chamber. The collecting length would be changed in a matter of minutes instead of hours, time needed to pressurise and make vacuum. This would lead to a large number of data sets with a wide range of different geometries that would serve to draw conclusions about the influence of the probe geometry on the results.

Also, the measurements must be performed at different plume regions in order to build the density and temperature structure within the thruster plasma plume. This can be easily done with a movable stand with remote control form outside the chamber.

Other open way regarding fabrication is the compensated Langmuir probe. It may be interesting to compare the results between the simple Langmuir probe and the compensated for the helicon thruster radio frequency plasma.

Regarding the processing of the data, more specific theories can be implemented to account more complex phenomena in a more detailed analysis of the plasma. Also creating faster and more automatic routines would imply more data analysed saving time to carefully process those sets that are difficult to auto-process.

About the results, it was seen that all the data sets obtained in the university facilities are similar between each other, and quite different to the Random Data curve. While this last presents a pure ideal IV curve, the exponential increases smoothly, all the curves measured here display a sudden steep increasing exponential before the floating potential. The reason for this fact is the low density of the plasma.

If a more exhaustive sweep throughout all the thruster regimes is carried out, it could be deduced more reliably the difference between both methods for the new conditions.

Finally, thinking even further, if a model of the plasma is designed, simulation on Langmuir probe theory could be carried out. Comparing the experimental results with the ones obtained from the theoretical model would enrich the theories about ion collection and even new approaches could be conceived to account for real effects.

Appendix A

Codes

The following appendix contains the codes implemented in Matlab (ref) and all the respective sub-functions.

- General Method

```
function [res, err, AuxParam]=postp_LP_General(Vdes, I, lp,  lr,  mi, const)
    ;
% ------------------Constants-------------------------
KB      = const.KB;    %[m^2 kg /( s^2 K^1 )], Boltzmann const
e       = const.e;    %[c], electron charge
me      = const.me;   %[kg], electron mass
ep0     = const.ep0;   %[F/m], Vacuum permittivity
% Probe collecting surface
S = 2*pi*lr*lp;
%% Floating potential
idx1 = find(I>0,1); % Index for floating potential
Vf = Vdes(idx1);
%% Plasma potential
% Variation of current wrt potential
DIDV = gradient(I(1:end-20), Vdes(1:end-20));
% First user interaction - plasma potential choice
    figure(10)
    plot(Vdes(idx1-20:end-20), DIDV(idx1-20:end))
    xlabel('Voltage [V]')
    ylabel('DI/DV [A/V]')
    grid minor
    title('Plasma potential selection - General method')
    hold on
[Vs,~] = ginput(1);
    line([Vs Vs], ylim,'color','r','linewidth',1,'linestyle','--')
    legend('DI/DV','Vs','Location','best')
%% Ion Saturation Range (until floating potential neighborhood)
% Ion range itself
V_ISrng = Vdes(1:idx1+20);
I_ISrng = I(1:idx1+20);
% Second user interaction - selection of ion range
```

```
    figure(11)
    subplot(2,1,1)
    h1=plot(V_ISrng,I_ISrng,'+-');
    hold on
    line(xlim, [0 0],'color','k','linewidth',0.75,'linestyle','--')
    line([0 0], ylim,'color','k','linewidth',0.75,'linestyle','--')
    grid minor
    title('Ion saturation range ( Ion fit ) - General method')
    xlabel('Voltage [V]')
    ylabel('Current [A]')
    zoom on;
    pause()
    zoom off;
LIM=xlim;
% Search for left limit
dif1=abs(V_ISrng-LIM(1));
idx2_i = find(dif1 == min(dif1));
% Search for right limit
dif2=abs(V_ISrng-LIM(2));
idx3_i = find(dif2 == min(dif2));
% Range to fit
xdata_i=V_ISrng(idx2_i:idx3_i);
ydata_i=I_ISrng(idx2_i:idx3_i);
    zoom out;
% Fit coefficients
ISRfit=polyfit(xdata_i,ydata_i,1);
% Linear error
ydatafit_i = ISRfit(1)*xdata_i+ISRfit(2);
err_if_linear_vect = abs(ydatafit_i-ydata_i)./abs(ydata_i)*100;
err_if_linear = mean(err_if_linear_vect);
% Constant error
ISRc = mean(ydata_i);
err_if_const_vect = abs(ydata_i-ISRc)./abs(ydata_i)*100;
err_if_const = mean(err_if_const_vect);
% Theoretical ion current
I_ISRfit=ISRfit(1)*Vdes+ISRfit(2);
Isat=ISRfit(1)*Vf+ISRfit(2); %Saturation ion current
    h2=plot(xdata_i,ydatafit_i,'r','Linewidth',2);
    h3=plot(Vdes,I_ISRfit,'r--','Linewidth',1.5);
    h4 = plot(Vf,Isat,'kx','Linewidth',1.5);
    legend([h1 h2 h3 h4],{'Data','Fit','Fit extrapolation','Saturation
    current'},'Location','best');
%Error subplot
    subplot(2,1,2)
    plot(xdata_i,err_if_linear_vect)
    hold on
    line(xlim, [err_if_linear err_if_linear],'color','b','linewidth',0.75,'
    linestyle','--') %x-axis
    plot(xdata_i,err_if_const_vect)
    line(xlim, [err_if_const err_if_const],'color','r','linewidth',0.75,'
    linestyle','--') %x-axis
    title('Ion fit errors')
    legend('Linear error','Linear error mean','Constant error','Constant
    error mean','Location','best')
    xlabel('Voltage fitting range [V]')
```

```
    ylabel('Error [%]')
    grid minor
% Auxiliar index to correct the ion current above the Vf
auxidx=find(I_ISRfit>0,1);
I_ISRfit(auxidx:end)=0;
Imod=I-I_ISRfit; % Substracted I
%%  Electron gain slope
idx1mod=find(Vdes>Vf-10,1);
V_ETslp=Vdes(idx1mod:end);
I_ETslp=Imod(idx1mod:end);
I_ETslp_woSB=I(idx1mod:end); % Current without substracting
%Semilog scale with plot
V_ETslp_smlg=V_ETslp;
I_ETslp_smlg=log(I_ETslp);
I_ETslp_woSB_smlg=log(I_ETslp_woSB);
% Manual selection of the range
    figure(12)
    subplot(2,1,1)
    plot(V_ETslp_smlg,I_ETslp_smlg,'+-')
    hold on
    plot(V_ETslp_smlg,I_ETslp_woSB_smlg,'g-')
    line([Vs Vs], ylim,'color','k','linewidth',0.5,'linestyle','--') %y-axis
    line([Vf Vf], ylim,'color','k','linewidth',0.5,'linestyle','-.') %y-axis
    grid minor
    title('Semilog for electron gain range ( Electron fit ) - General method
    ')
    xlabel('Voltage [V]')
    ylabel('Log(I) [A]')
    legend('Data','Data wo subst.','location','best')
    zoom on;
    pause()
    zoom off;
LIM=xlim;
% Search for left limit
dif1=abs(V_ETslp_smlg-LIM(1));
idx2 = find(dif1 == min(dif1));
% Search for right limit
dif2=abs(V_ETslp_smlg-LIM(2));
idx3 = find(dif2 == min(dif2));
% Range to fit
xdata=V_ETslp_smlg(idx2:idx3);
ydata=I_ETslp_smlg(idx2:idx3);
    zoom out;
% Electron fit coefficients
EGfit=polyfit(xdata,ydata,1);
% Electron temperature
Te_B=1/EGfit(1); %[eV]
    hold on
ydatafit=xdata*EGfit(1)+EGfit(2);
    plot(xdata,ydatafit,'r--','Linewidth',2)
    legend('Data','Data wo subst.','Vs','Fit','Location','best')
    err_ef_vector=abs(ydata-ydatafit)./abs(ydata)*100;
    err_ef=mean(err_ef_vector);
    subplot(2,1,2)
    plot(xdata,err_ef_vector)
```

```
    hold on
    line(xlim, [err_ef err_ef],'color','b','linewidth',0.75,'linestyle','--'
    ) %x-axis
    title('Error of Electron fit')
    xlabel('Voltage [V]')
    ylabel('Error of log [%]')
    legend('Error','Error mean','Location','best')
    grid minor
%% Parameters
Isat=-abs(ISRfit(1)*Vf+ISRfit(2));      % Saturation ion current [A]
ni=-Isat/(0.6*e*S)*sqrt(mi/(e*Te_B));   % Ion density [m^-3]
DL=sqrt(ep0*Te_B/ni/e);                 % Debye length [m]
%% Outputs
res = [Te_B, ni,Vs,Vf]; % Results for parameters
err = [NaN, err_if_linear, err_if_const, err_ef]; % Errors
AuxParam = [Vdes(idx2_i) Vdes(idx3_i) -ISRfit(1)/Isat];
% Auxiliar parameters with more information about the fits:
%[left ion limit, right ion limit, slope ion fit
%% Printing of the results
    display(' - General method -')
    display('Values found:')
    display(['    - Electron temperature : ',num2str(res(1)),' eV'])
    display(['    - Plasma density : ',num2str(res(2),'%10.3e'),' m^-3'])
    %display(['    - Debye length: ',num2str(res(3),'%10.3e'),' m'])
    display(['    - Floating potential: ',num2str(res(4)),' V'])
    display(['    - Plasma potential: ',num2str(res(3)),' V',char(10)])
    display(['Ion linear fit mean error : ', num2str(err_if_linear),' %'])
    display(['Ion constant fit mean error : ', num2str(err_if_const),' %'])
    display(['Electron fit mean error : ', num2str(err_ef),' %'])
end
```

- EPFL Method

```
function [res, err, AuxParam] = postp_LP_epfl(Vdes, I, lp,  lr,  mi, const);
% ------------------Constants-------------------------
KB      = const.KB;    %[m^2 kg /( s^2 K^1 )], Boltzmann const
e       = const.e;    %[c], electron charge
me      = const.me;   %[kg], electron mass
ep0     = const.ep0;   %[F/m], Vacuum permittivity
% Probe collecting surface
S = 2*pi*lr*lp;
%% Floating potential
idx1 = find(I>0,1); % Index for floating potential
Vf = Vdes(idx1);
%% Plasma potential
% Variation of current wrt potential
DIDV = gradient(I(1:end-20), Vdes(1:end-20));
% 1st user interaction
    figure(20)
    plot(Vdes(idx_vf-20:end-20), DIDV(idx_vf-20:end))
    xlabel('Voltage [ V ]')
    ylabel('DI/DV [ A/V ]')
    title('Plasma potential selection - EPFL method')
    grid minor
    hold on
```

```
[Vs,~] = ginput(1);
idx_vs=find(Vdes-Vs>0,1);
    line([Vs Vs], ylim,'color','r','linewidth',1,'linestyle','--') %x-axis
    legend('DI/DV','Vs','Location','best')
%% Overall range
    figure(21)
    h1=plot(Vdes,I,'+-');
    hold on
    line(xlim, [0 0],'color','k','linewidth',0.75,'linestyle','--') %x-axis
    line([0 0], ylim,'color','k','linewidth',0.75,'linestyle','--') %y-axis
    grid minor
    title('Overall fitting range - EPFL method')
    xlabel('Voltage [ V ]')
    ylabel('Current [ A ]')
[Vl_ionrng,~] = ginput(1); % Input of lower bound of range
    h2=line([Vl_ionrng Vl_ionrng], ylim,'color','r','linewidth',1,'linestyle
    ','--'); %x-axis
    h3=line([Vs Vs], ylim,'linewidth',0.5,'linestyle','-.'); %x-axis
    h4=line([Vf Vf], ylim,'color','g','linewidth',0.5,'linestyle','-.'); %x-
    axis
%legend([h1 h2 h3],{'Data','Lower limit','Upper limit (Plasma Potential)'},'
    Location','best')
idx_l_ionrng=find(Vdes-Vl_ionrng>0,1);
% Calculation of initial guesses
Auto_AlphaGuess=-I(idx_l_ionrng)/(Vf-Vdes(idx_l_ionrng))/1e-5;
Auto_TeGuess = abs(I(idx_vs)/DIDV(idx_vs));
Auto_IsatGuess = I(idx_vs)/(1-Auto_AlphaGuess*(Vs-Vf)-exp((Vs-Vf)/
    Auto_TeGuess));
% Initial guesses structure
InitGuess=[Auto_IsatGuess Auto_TeGuess Auto_AlphaGuess];
% Definition of functions for fitting
for i=1:idx_vs-idx_vf
I2fit=I(idx_l_ionrng:i+idx_vf);
Vfit=Vdes(idx_l_ionrng:i+idx_vf);
fun_overall_fit = @(x) x(1)*(1-x(3)*(Vfit-Vf)-exp((Vfit-Vf)/x(2)));
funERR = @(x) sum(abs((fun_overall_fit(x))-(I2fit)));
[AUX]=fminsearch(funERR,InitGuess);
AUXvec(i)=AUX(2);
end
minTe_i=find(min(AUXvec)==AUXvec);
idx_upper_l=idx_vf+minTe_i;
% Range of the overall fit
I2fit=I(idx_l_ionrng:idx_upper_l);
Vfit=Vdes(idx_l_ionrng:idx_upper_l);
Vdec=Vfit(end); % Potential from Minimum Temperature Method
% Definition of fitting function
fun_overall_fit = @(x) x(1)*(1-x(3)*(Vfit-Vf)-exp((Vfit-Vf)/x(2)));
funERR = @(x) sum(abs((fun_overall_fit(x))-(I2fit)));
% Fit
[Param,extra]=fminsearch(funERR,InitGuess);
% Theoretical total current
Ifit=fun_overall_fit(Param);
%Ifit2=fun_overall_fit(InitGuess); %Initial guess current
% Error calculation
err_overallfit_vect=abs(I2fit-Ifit)./abs(I2fit)*100;
```

```
err_overallfit=mean(err_overallfit_vect);
    h5=plot(Vfit,Ifit,'-m','Linewidth',1.5);
    %h6=plot(Vfit,Ifit2,'-k','Linewidth',1);
    h7=line([Vdec Vdec], ylim,'linewidth',1,'linestyle','--');
    legend([h1 h5 h2 h7 h3 h4],{'Data','Fit','Lower limit','Upper limit (Min
    . Te)','Plasma potential','Floating potential'},'Location','best')
    xlim([Vl_ionrng-15 Vs+15])
    ylim([Ifit(1)*1.5 Ifit(end)*2])
%% Parameters
Isat=Param(1);                          % Saturation ion current [A]
Te=Param(2);                            % Electron temperature [eV]
ni=-Isat/(0.6*e*S)*sqrt(mi/(e*Te));     % Ion density [m^-3]
DL=sqrt(ep0*Te_B/ni/e);                 % Debye length [m]
%% Outputs
res = [Te, ni,Vs,Vf]; % Results for parameters
err = [err_overallfit]; % Errors
AuxParam = [Vl_ionrng Param(3) Vdec];
% Auxiliar parameters with more information about the fits:
%[lower overall range limit, alpha from fit, potential for the lowest Te]
%% Printing of the results
display(char(10))
display(' - EPFL method -')
display('Values found:')
display(['    - Electron temperature : ',num2str(res(1)),' eV'])
display(['    - Plasma density : ',num2str(res(2),'%10.3e'),' m^-3'])
% display(['    - Debye length: ',num2str(res(3),'%10.3e'),' m'])
display(['    - Floating potential: ',num2str(res(4)),' V'])
display(['    - Plasma potential: ',num2str(res(3)),' V',char(10)])
display(['Overall fit error : ', num2str(err_overallfit),' %'])
end
```

- Comparison function

```
function  method_compare
clc
close all
clear all
%% General Data
flg_p = 4;
% probe: 1->A, 2->B, 3->C, 4->April
flg_g = 2;
% Gas Type: 1->Xenon; 2->Argon
Resistance = 0; %[Ohms] or 0.
% 0 -> Kithley; Ohms for DAQ resistance.
% 1e3; % April data
% ------------------Constants--------------------------
KB      = 1.38064852e-23;    %[m^2 kg /( s^2 K^1 )], Boltzmann const
e       = 1.60217662e-19;    %[c], electron charge
me      = 9.109382910e-31;   %[kg], electron mass
ep0     = 8.854187817e-12;   %[F/m], Vacuum permittivity
u_mass  = 1.660539040e-27;   %[kg], atomic mass unit
% Structure for constants
const = struct('KB', KB, 'e', e,'me', me, 'ep0', ep0);
% ----------------Probe Geometry--------------------------
% June Helicon
```

```
if flg_p == 1 %probe A
    lp = 5e-3;                  %[m] length
    lr = 1.27e-4/2;             %[m] radius
elseif flg_p == 2 % probe B
    lp = 3e-3;                  %[m] length
    lr = 1.27e-4/2;             %[m] radius
elseif flg_p == 3 % pribe C
    lp = 3e-3;                  %[m] length
    lr = 1.27e-4;               %[m] radius
elseif flg_p == 4 % April
    lp = 2e-3;                  %[m] length
    lr = 1.25e-4;               %[m] radius
end
% ------------------Gas Type-------------------------
if flg_g==1
    % Gas type xenon
    mi = 131.293*u_mass;        %[kg]
elseif flg_g == 2
    % Gas type argon
    mi = 39.948*u_mass;         %[kg]
end

%% Input Data process
 Datanum = 4; %Out of 4
 [V, I] = inIV_Random(Datanum); % Random data

%  [V, I,DataName] = inIV_Jun; % june Helicon data
 %% Subtract end effects
I =  subt_end(V, I, lp, lr);
%%
% Collecting probe area
S=2*pi*lr*lp;
% Floating potential
idx_vf=find(I>0,1); % index of Vf
Vf=V(idx_vf);
% Definition of fitting function
fun_overall_fit = @(x,xdata) x(1)*(1-x(3)*(xdata-Vf)-exp((xdata-Vf)/x(2)));
% Running of methods to compare
[res_G, err_G, AuxParam_G] = postp_LP_General(V, I, lp,  lr,  mi, const);
Isat_G = -res_G(2)*(0.6*e*S)/sqrt(mi/(e*res_G(1)));
[res_E, err_E, AuxParam_E] = postp_LP_epfl(V, I, lp,  lr,  mi, const);
Isat_E = -res_E(2)*(0.6*e*S)/sqrt(mi/(e*res_E(1)));
% [res_C, err_C]=postp_LP_chen2001_v2(V, I, lp,  lr,  mi, const, res_G)
% Isat_C = -res_C(2)*(0.6*e*S)/sqrt(mi/(e*res_C(1)));
%% Bounds for fitting range
% Upper limit
V_upb = (AuxParam_E(3));
idx_upb = find(V-V_upb>0,1);
V_upb = V(idx_upb);
% Lower limit
V_lowb=(AuxParam_G(1)+AuxParam_E(1))/2;
idx_lowb = find(V-V_lowb>0,1);
V_lowb = V(idx_lowb);
% Plasma potential
Vs = (res_G(3)+res_E(3))/2;
```

```
idx_vs= find(V-Vs>0,1);
%Range to evaluate
Imod = I(idx_lowb:idx_upb);
Vmod = V(idx_lowb:idx_upb);
% Evaluation of the methods
I_G = fun_overall_fit([Isat_G res_G(1) AuxParam_G(3)],Vmod);    %General
    Method
I_E = fun_overall_fit([Isat_E res_E(1) AuxParam_E(2)],Vmod);    %EPFL Method
% I_C = fun_overall_fit([Isat_C res_C(1) AuxParam_C(2)],Vmod);
    figure(30)
    plot(V,I,'+')
    xlabel('Voltage [ V ]')
    ylabel('Current [ A ]')
    title('Comparison of post-process methods')
    grid minor
    hold on
    plot(Vmod,I_E,'--g','Linewidth',2);
    plot(Vmod,I_G,'--m','Linewidth',2);
    % plot(Vmod,I_C,'--c','Linewidth',2);
    line([V_lowb V_lowb], ylim,'color','b','linewidth',0.5,'linestyle','--')
    line([V_upb V_upb], ylim,'color','k','linewidth',0.5,'linestyle','--')
    legend('Data','EPFL method','General method','Lower limit','Upper limit'
    ,'location','best')
    xlim([V_lowb-15 V_upb+15])
    ylim([min(I_E(1)*1.5,I_G(1)*1.5) max(I_E(end)*1.5,I_G(end)*1.5)])
%% Errors
% EPFL method
err_E_fit_vec=abs(Imod-I_E)./abs(Imod)*100;
err_E_fit_vec=[err_E_fit_vec(1:idx_vf-idx_lowb-1)  err_E_fit_vec(idx_vf-
    idx_lowb+2:end)];
err_E_fit=mean(err_E_fit_vec);
% General method
err_G_fit_vec=abs(Imod-I_G)./abs(Imod)*100;
err_G_fit_vec=[err_G_fit_vec(1:idx_vf-idx_lowb-1)  err_G_fit_vec(idx_vf-
    idx_lowb+2:end)];
err_G_fit=mean(err_G_fit_vec);
% Chen2001
% err_C_fit_vec=abs(Imod-I_C)./abs(Imod)*100;
% err_C_fit=mean(err_C_fit_vec);
    figure(31)
    plot([Vmod(1:idx_vf-idx_lowb-1)  Vmod(idx_vf-idx_lowb+2:end)] ,
    err_E_fit_vec,'*g','linewidth',0.5);
    hold on
    grid minor
    plot([Vmod(1:idx_vf-idx_lowb-1)  Vmod(idx_vf-idx_lowb+2:end)],
    err_G_fit_vec,'*r','linewidth',0.5);
    % plot(Vmod,err_C_fit_vec,'*r','linewidth',0.5);
    ylim([ -err_G_fit 5*err_G_fit])
    line(xlim, [err_E_fit err_E_fit],'color','g','linewidth',0.5,'linestyle'
    ,'--')
    line(xlim, [err_G_fit err_G_fit],'color','r','linewidth',0.5,'linestyle'
    ,'--')
    line([Vf Vf], ylim,'color','k','linewidth',0.25)
    line(xlim, [0 0],'color','k','linewidth',0.5,'linestyle','--','Color'
    ,[0.4,0.4,0.4])
```

```
    legend('EPFL method error','General method error',['EPFL method mean
    error : ',num2str(err_E_fit),' %'],['General method mean error : ',
    num2str(err_G_fit),' %'],'Floating potential','Location','best')
    xlabel('Voltage [ V ]')
    ylabel('Error [%]')
    title('Error of post-process methods wrt data')
%% Saving graphs procedure
 GraphNames={'Vplas_General','IonRange_General','ElecRange_General','
    Vplas_EPFL','TotalFit_EPFL','Compare','ErrorComp'};
 GraphIndex=[10 11 12 20 21 30 31];
    for k=1:numel(GraphNames);
        fpath='C:\Users\Gabriel\Downloads\PLASMA GRAPHS compareR';
        filenameg=[['Data' num2str(Datanum) '_'] GraphNames{k}];
%         filenameg=[DataName{1} '_' GraphNames{k}];
        saveas(GraphIndex(k),fullfile(fpath,filenameg),'png')
    end
RESULTS=[res_G ; res_E ];
filenamer=['RESULTS_' 'Data' num2str(Datanum) '.txt'];
% filenamer=['RESULTS_' DataName{1} '.txt'];
save(fullfile(fpath,filenamer),'RESULTS','-ascii')
end
```

- Chen2001 Algorithm

```
function [res, err]=postp_LP_chen2001(V, I, lp,  lr,  mi, const, VarGuess)
%% Iterations
global PreVal   Errors
PreVal=[0; 0; 0; 0];
GenData=[const.KB,const.e,const.ep0,lr,lp,mi,const.me];
% options = optimset('Display','iter','PlotFcns',@optimplotx);
[FinVal,fval]=fminsearch(@(InVal) OPT(InVal,GenData,I,V),VarGuess);%,options
    );
% Output Data
Te      =   FinVal(1);
ne      =   FinVal(2);
Vs_e    =   FinVal(3);
Vs_i    =   FinVal(4);
err_f   =   fval;
err_if  =   Errors(1);
err_ef  =   Errors(2);
% Standard structure
res = [Te, ne, Vs_e, Vs_i];
err = [err_f, err_if, err_ef];
%% Display Results
display('Initial guesses:')
display(['    - Electron temperature : ',num2str(VarGuess(1)),' eV'])
display(['    - Plasma density : ',num2str(VarGuess(2),'%2.2e'),' m^-3'])
display(['    - Electron plasma potential: ',num2str(VarGuess(3)),' V'])
display(['    - Ion plasma potential: ',num2str(VarGuess(4)),' V',char(10)])
display('Values found:')
display(['    - Electron temperature : ',num2str(Te),' eV'])
display(['    - Plasma density : ',num2str(ne,'%10.3e'),' m^-3'])
display(['    - Electron plasma potential: ',num2str(Vs_e),' V'])
display(['    - Ion plasma potential: ',num2str(Vs_i),' V',char(10)])
display(['Error function value : ', num2str(fval)])
```

```
display(['Ion fit error : ', num2str(err_if)])
display(['Electron fit error : ', num2str(err_ef)])
end


function error =OPT(InVal,GenData,I,V)
global PreVal Errors
[FinVal,Errors]=EstimPlasmParam(InVal,GenData,V,I);
% Definition of global error
error=sum(Errors)*1e3;
% Other error approach
% error=sum((FinVal-PreVal)./PreVal)*1e3;
PreVal=FinVal;
end


function [FinVal,Errors] = EstimPlasmParam(InVal,GenData,V,I)
persistent flg_isub
% Input parameters
Te=InVal(1) ;% Te in eV
n=InVal(2);
Vse=InVal(3);
Vsi=InVal(4);
% Input General Data
KB=GenData(1);
e=GenData(2);
ep0=GenData(3);
lr=GenData(4);
lp=GenData(5);
mi=GenData(6);
me=GenData(7);
% Non-dimenional current
Ap=2*pi*lr*lp;              % Collection surface
Jr=e*Ap*sqrt(e*Te/2/mi/pi); % Reference non-dimensional current
IonData=[Jr,lr,e,ep0];
ind_se  = find(V>Vse,1)-1;
% options = optimset('Display','iter','PlotFcns',@optimplotx);
if isempty(flg_isub)
    flg_isub = 1;
    [FinIonVars,fvalION]=fminsearch(@(IonVars) IonFitERR(IonVars,I,V,Te,
    IonData),[n Vsi]);
else
    f_Iefit = @(vec) (n*e*Ap*(e*vec(1)/2/pi/me).^0.5.*exp((V-vec(2))./vec(1)
    ));
    Ie_2sub = f_Iefit([Te Vse]);
    Ie_2sub(ind_se:end) = 0 ;
    Ii_sub  = I - Ie_2sub;
    [FinIonVars,fvalION]=fminsearch(@(IonVars) IonFitERR(IonVars,Ii_sub,V,Te
    ,IonData),[n Vsi]);
end
% Output from optimization
nnew=FinIonVars(1);
Vsi=FinIonVars(2);
% Performing of the ion fit
[~, inew] = IonFitERR(FinIonVars,I,V,Te,IonData);
```

```
ind_si = find(V>Vsi,1); % Plasma potential
inew(ind_si:end)=0;
Iinew=nnew*Jr*inew; % Ion current, to be shortened
Ie=I+Iinew;
% Values found
FinVal(2,1)=nnew; % Plasma density
FinVal(4,1)=Vsi;  % Ion plasma potential
%% STEP 7 & 8
% Indexes
ind_f  = find(I>0,1); % Floating potential
ind_min = ind_f+10;
ind_max = max(ind_se, ind_f);
% Range to fit
xdata = V(ind_min:ind_max);
ydata = Ie(ind_min:ind_max);
% Definition for the fitting functions
f_Iefit = @(vec) (nnew*e*Ap*(e*vec(1)/2/pi/me).^0.5.*exp((xdata-vec(2))./vec
    (1)));
funERR  = @(vec) sum(abs((f_Iefit(vec)*1e6).^2-(ydata*1e6).^2));
[vecnew,fvalELEC]=fminsearch(funERR,[Te Vse]);
% Calculated electron current
Iefit = f_Iefit(vecnew);
ind_p = [min(ind_f,ind_si):max([ind_f ind_si  ind_se])];
% Values found
FinVal(1,1)=vecnew(1); % Electron temperature
FinVal(3,1)=vecnew(2); % Electron plasma potential
% Errors from fit
Errors=[fvalION fvalELEC];
end


function [ERR,ifit] =IonFitERR(IonVars,I,V,Te,IonData)
% This function is in charge of performing the ion fit for the Chen2001
% algorithm.
% Input Data
Jr=IonData(1); % Non-dimensional reference current
lr=IonData(2); % Probe length
e=IonData(3);  % Electron charge
ep0=IonData(4);% Vacuum permeability
mi = 39.948*1.660539040e-27; % Ion mass [kg]
me = 9.109382910e-31;        % Electron mass [kg]
Vsi=IonVars(2); % Ion plasma potential
n=IonVars(1);   % Plasma density
% Non-dimensional potential
DL = sqrt(ep0*Te/n/e); % Debye length
xi = lr/DL;
eta   = (Vsi-V)/Te;
% Indexes
ind_s = find(eta<0,1)-1; % plasma potential index
ind_f = find(I>0,1)-1; % floating potential index
% Fitting of parameters
    if xi>3
        %Eq. 9 - Table II
        funA=@(q) q(1)+q(2)*(xi-q(3)).^q(4).*exp(-q(5)*(xi-q(3)).^q(6));
        funB=funA;
```

```
        funC=@(q) q(1)+q(2)*exp(-q(3)*log(xi-q(4)))+q(5)*(1-q(6)*log(xi));
        funD=funA;
        coefs=[1.142 19.027 3     1.433  4.164 0.252
               0.53  0.97   3     1.11   2.12  0.35
               0     1      3     1.95   1.27  0.035
               0     2.65   2.96  0.376  1.94  0.234];
    else
        %Eq. 10 - Table IV
        funA=@(q) q(1)+1./(1/q(2)./xi.^q(3)-1/q(4)./log(xi/q(5)));
        funB=@(q) q(1)+q(2)*xi.^q(3).*exp(-q(4)*xi.^q(5));
        funC=@(q) q(1)+q(2)*xi.^-q(3);
        funD=funB;
        coefs=[1.12    0.00034 6.87   0.145    110
               0.5     0.008   1.5    0.18     0.8
               1.07    0.95    1.01   0        0
               0.05    1.54    0.3    1.135    0.37];
    end
% Coefficients
    A=funA(coefs(1,:));
    B=funB(coefs(2,:));
    C=funC(coefs(3,:));
    D=funD(coefs(4,:));
%% Saturation ion region (lower than Vs)
ifit=((A*abs(eta).^B).^-4+(C*abs(eta).^D).^-4).^-0.25;
ifit(ind_s+1:end)=-ifit(ind_s+1:end)*sqrt(mi/me);
% V > 0, electron OM current
idata = - I/(Jr*n);
idata(ind_f+1:end)=0; % Correction
% Fitting indexes
ind_min = find(V>-50,1);
ind_max = ind_f+10;
ind_p = max(ind_f,ind_s);
% Definition of error function
ERR = sum(abs(ifit(ind_min:ind_max)-idata(ind_min:ind_max)));
% %%%%%%%%%%%%%%%%%%%%%%%
% %Set Vmin Vmax for ion fitting
% %%%%%%%%%%%%%%%%%%%%%%%
% % if Vsi<27
% %     ERR=inf;
% % else
% ERR= sum(abs(Ip.^2-(inp*Jr*n).^2));
% end
end
```

Bibliography

[Bernstein and Rabinowitz, 1959] Bernstein, I. B. and Rabinowitz, I. N. (1959). Theory of electrostatic probes in a low-density plasma. *Physics of Fluids (1958-1988)*, 2(2):112–121.

[Chen, 2001] Chen, F. F. (2001). Langmuir probe analysis for high density plasmas. *Physics of Plasmas (1994-present)*, 8(6):3029–3041.

[Chen et al., 1965] Chen, F. F., Evans, J. D., and Zawalski, W. (1965). Electric probes. In *In Plasma Diagnostic Techniques, edited by Huddlestone, RH and Leornard, SL*. Citeseer.

[Conde, 2011] Conde, L. (2011). An introduction to langmuir probe diagnostics of plasmas. *Madrid: Dept. Física. ETSI Aeronáut ngenieros Aeronáuticos Universidad Politécnica de Madrid*.

[F.F.Chen] F.F.Chen. Low temperature plasma technology laboratory, university of california. `http://www.seas.ucla.edu/ltptl/presentations.htm`. Accessed: 2016-04-24.

[Furno, 2012] Furno, I. (2012). Theory of electrostatic probes. Education slides.

[Goldston and Rutherford, 1995] Goldston, R. J. and Rutherford, P. H. (1995). *Introduction to plasma physics*. CRC Press.

[Hershkowitz, 2013] Hershkowitz, N. (2013). 3 how langmuir probes work. *Plasma Diagnostics: Discharge Parameters and Chemistry*, 1:113.

[Hutchinson, 2002] Hutchinson, I. H. (2002). Principles of plasma diagnostics: Second edition. *Plasma Physics and Controlled Fusion*, 44(12):2603.

[KEITHLEY] KEITHLEY. Model 6517b electrometer.

[Laframboise, 1966] Laframboise, J. G. (1966). Theory of spherical and cylindrical langmuir probes in a collisionless, maxwellian plasma at rest. Technical report, DTIC Document.

[Langmuir, 1960] Langmuir, I. (1960). *The Collected Works of Irving Langmuir: Heat transfer. Incandescent tungsten*, volume 2. Published with the editorial assistance of the General Electric Company by Pergamon Press.

[Mathworks] Mathworks. Matlab r2015a. `http://es.mathworks.com/products/matlab/`.

[Merlino, 2007] Merlino, R. L. (2007). Understanding langmuir probe current-voltage characteristics. *American Journal of Physics*, 75(12):1078–1085.

[Miyamoto, 1997] Miyamoto, K. (1997). *Fundamentals of plasma physics and controlled fusion*. Iwanami Book Service Center.

[Mott-Smith and Langmuir, 1926] Mott-Smith, H. M. and Langmuir, I. (1926). The theory of collectors in gaseous discharges. *Physical review*, 28(4):727.

[Navarro-Cavallé et al., 2013] Navarro-Cavallé, J., Ahedo, E., Merino, M., Gómez, V., and Ruiz, M. (2013). Helicon plasma thrusters: prototypes and advances on modeling.

[Schrittwieser et al., 2005] Schrittwieser, R., Ionita, C., Balan, P., Varandas, C., Figueiredo, H., Stockel, J., Adámek, J., Hron, M., Ryszawy, J., and Tichy, M. (2005). Probe methods for direct measurements of the plasma potential. *Romanian Journal of Physics*, 50(7/8):723.

[Sudit and Chen, 1994] Sudit, I. D. and Chen, F. F. (1994). Rf compensated probes for high-density discharges. *Plasma Sources Science and Technology*, 3(2):162.

[Tejero del Caz, 2016] Tejero del Caz, A. (2016). *Análisis teórico del contacto plasma superficie y sus aplicaciones industriales*. PhD thesis, Universidad de Córdoba.

[University of Michigan] University of Michigan, D. o. A. E. Plasma diagnostics - langmuir probe. `http://pepl.engin.umich.edu/diagnostics/langmuir.html`. Accessed: 2016-05-30.